ENGINEERING RESEARCH INSTITUTE
THE UNIVERSITY OF MICHIGAN
ANN ARBOR

Final Report

SUPERSONIC MIXING OF JETS AND TURBULENT BOUNDARY LAYERS

WADC Technical Report No. 57-402

Harry E. Bailey
Arnold M. Kuethe

Department of Aeronautical Engineering

Project 2270

DEPARTMENT OF THE AIR FORCE
WRIGHT AIR DEVELOPMENT CENTER
WRIGHT-PATTERSON AIR FORCE BASE, OHIO
CONTRACT NO. AF 33(616)-2403
PROJECT NO. 54-610-185

June 1957

ACKNOWLEDGEMENTS

The authors gratefully acknowledge the financial support of Wright Air Development Center and the advice and assistance of the following persons. Professor S. I. Cheng of Princeton University spent two months in the summer of 1956 making a theoretical study (Reference 12) of supersonic mixing. Dr. Hans Wittenberg of Delft Technical Institute, Holland, also spent the summer of 1956 on this work. Mr. Bruce Nordquist, who was employed on a grant from the General Electric Company to further this work, assisted in making many of the measurements.

TABLE OF CONTENTS

LIST OF FIGURES

ABSTRACT

A theory is presented which permits the solution of a linearized form of the momentum equation for the case of two flows at different Mach numbers which merge as at the trailing edge of a two-dimensional airfoil. For the case of Prandtl number equal to one, it is shown that the energy equation reduces to the same form as the momentum equation.

The theoretical solutions which are obtained for the velocity distribution in the mixing region are compared with experimental measurements made in a special supersonic channel.

OBJECTIVE

The aim of the present work on supersonic jet mixing was to determine the effects of various factors such as Mach number, Reynolds number, and initial boundary-layer thickness on the mixing process.

I. INTRODUCTION

The flow over supersonic aircraft contains regions in which two streams of different Mach number and pressure come into contact with each other. Flow aft of the trailing edges of wings and at the exit of the propulsion device are the most common examples.

In subsonic flow the rate of mixing of two streams is quite well known.[1] It is fairly rapid compared with the rates encountered for supersonic streams. The present work constitutes a detailed study of total head and total temperature traverses in a special supersonic channel in which two streams of different Mach numbers and pressures merge.

II. THEORY OF COMPRESSIBLE TURBULENT MIXING

Many analyses of turbulent mixing, all of them phenomenological, have appeared since the first analysis by Tollmien[2] using Prandtl's mixing-length concept. All the theories involve assumptions and approximations, most of which cannot be segregated, so that a theory either agrees or does not agree with experiment; if it does not, the point of breakdown of the theory cannot in general be determined because of the number of simplifications which have been introduced.

Perhaps the simplest theories available are those proposed by Prandtl and Reichardt,[3,4] as a result of which the momentum equation takes the form of the heat-conduction equation. With similar simplifications and Prandtl number equal to unity, the energy equation also reduces to the heat-conduction equation with the stagnation temperature as the dependent variable. The theories contain two parameters, one of which must be evaluated from the observed rate of spread of the mixing region, and the other establishing the origin of the coordinate system.

Surprisingly, the superposition of effects implied by the linearity of the differential equations appears to be borne out in practice, for those cases which have been investigated.[5] Chapman and Korst,[6] for instance, investigated the mixing of a compressible jet with still air, and Weinstein[7] investigated the mixing of a low-speed jet in a moving stream. In both experiments, superposition appears to be realized.

The present study is a severe test of superposition because the initial boundary layers are thick, and there is a strong gradient of static temperature normal to the flow. In the above references, neither the boundary layer nor compressibility effects were large, so the results were not a very rigorous test of the superposition principle.

In a mixing region, it is standard practice to adopt Prandtl's boundary-layer approximations, to neglect all pressure gradients, and to assume that viscosity is constant. Therefore, the equation of motion takes the form:

$$\frac{\partial u}{\partial t} + u \frac{\partial u}{\partial x} + v \frac{\partial u}{\partial y} = \nu \frac{\partial^2 u}{\partial y^2} \quad , \tag{1}$$

where u and v are instantaneous velocities, and $\nu = \mu/\rho$ is the kinematic viscosity. Let $u = U + u'$, where U is the mean velocity with time and u' is the velocity fluctuation. Similarly, $v = V + v'$. Then Equation 1 becomes, after taking mean values,

$$U \frac{\partial U}{\partial x} + V \frac{\partial U}{\partial y} = \frac{1}{\rho} \frac{\partial}{\partial y} \left[\mu \frac{\partial U}{\partial y} - \rho \overline{u'v'} \right] - \frac{1}{\rho} \frac{\partial}{\partial x} (\rho \overline{u'^2}) \quad , \tag{2}$$

where the bar signifies mean value with time. In this theory, variations and fluctuations in density are neglected.

Equation 2 has been simplified in two ways. In both ways, the terms

$$V \frac{\partial U}{\partial y} \quad , \quad \frac{\partial}{\partial x} (\rho \overline{u'^2})$$

and the laminar friction term $\mu \partial U/\partial y$ are neglected. Then, Equation 2 becomes

$$U \frac{\partial U}{\partial x} = - \frac{1}{\rho} \frac{\partial}{\partial y} (\rho \overline{u'v'}) \quad . \tag{3}$$

Now, $-\rho \overline{u'v'}$ is the Reynold's stress in the xy plane. Reichardt[4] approximates it by setting

$$\rho \overline{u'v'} = -\Lambda \frac{\partial (U^2)}{\partial y} \quad , \tag{3a}$$

and Equation 2 becomes

$$\frac{\partial (U^2)}{\partial x} = \frac{2\Lambda}{\rho} \frac{\partial^2 (U^2)}{\partial y^2} \quad , \tag{4}$$

where Λ is a mixing coefficient to be evaluated from experiment. This is the final form of the differential equation used in References 5 and 7 for incompressible jets.

Chapman and Korst, following Pai,[8] use a different linearization of Equation 2. They write, instead of Equation 3a,

$$\rho \overline{u'v'} = - \rho \epsilon \frac{\partial U}{\partial y} \quad , \tag{5}$$

and, instead of $U \partial U/\partial x$, they write

$$\frac{U_1 + U_2}{2} \frac{\partial U}{\partial x} \quad ,$$

i.e., they replace U by the average value of the two streams (Figure 1), thus assuming that the variation of U is small. Then Equation 2 becomes

$$\frac{\partial U}{\partial x} = \frac{2\epsilon}{\rho (U_1 + U_2)} \frac{\partial^2 U}{\partial y^2} \quad . \tag{6}$$

Equations 4 and 6 are of the same form, the coefficients on the right being assumed to be functions only of x, U_2/U_1, and possibly M_2/M_1. Whichever differential equation is used, the boundary conditions on U and U^2 will be similar. From here on we work with Equation 6, but the results are equally applicable to Equation 4, and at this point we cannot predict which, if either, will describe better the experimental results.

Korst, Page, and Childs[9] write the solution of Equation 6 for the mixing of a compressible fluid with still air. In the following, we extend their results to the mixing of two streams as shown in Figure 1.

The two streams have different supersonic Mach numbers (M_{1_o} and M_{2_o}), static pressures (p_1 and p_2), velocities (U_{1_o} and U_{2_o}), boundary-layer thicknesses (δ_1 and δ_2), and stagnation temperatures (T_{o_1} and T_{o_2}). The two streams merge at the lip, and aft of any shocks and expansions the ambient pressures become p_a and the directions of the two streams are again parallel, making an angle with their original directions determined by the ratio of their original ambient pressures. The initial conditions for the mixing are taken, as shown in Figure 1, at the lip. We write

$$\zeta = \frac{y}{\delta_2} \; ; \quad \psi = \frac{x}{\delta_2} \; ; \quad \Phi = \frac{U}{U_2} \; ; \quad \lambda = \frac{U_1}{U_2} \; .$$

Then Equation 6 becomes

$$\frac{\partial \Phi}{\partial \psi} = \frac{2\epsilon}{\rho U_2 \delta_2 (\lambda + 1)} \frac{\partial^2 \Phi}{\partial \zeta^2} \; . \tag{7}$$

Now, write

$$\epsilon = c\psi\delta_2 U_2 \frac{\lambda + 1}{2} \rho \, f(\psi) \; . \tag{8}$$

In Reichardt's analysis[4] ϵ is taken proportional to x for the case of $\delta_1 = \delta_2 = 0$. Korst, Page, and Childs[9] insert $f(\psi)$ in Equation 8 and this analysis approaches Reichardt's at a great distance from the lip if we postulate that $f(\psi) \to 1$ as $\psi \to \infty$. Let

$$\xi = \xi(\psi) = c \int_0^{\psi} \psi \, f(\psi) \, d\psi \; , \tag{9}$$

where c is a constant to be determined. Then

$$\frac{\partial}{\partial \psi} = c \, \psi \, f(\psi) \frac{\partial}{\partial \xi} \; ,$$

and Equation 7 becomes

$$\frac{\partial \Phi}{\partial \xi} = \frac{\partial^2 \Phi}{\partial \zeta^2} \; . \tag{10}$$

Equation 10 is the differential equation for heat conduction with unit transfer coefficient. The solution of that equation for the proper boundary conditions becomes immediately applicable to the mixing problem.

In terms of the physical variables, the initial conditions at $\psi = 0$ are:

$$y \leq -\delta_1 \ , \quad U = U_1 \qquad 0 < y < \delta_2 \ , \quad U = U_2\Phi_2(y)$$

$$y \geq \delta_2 \ , \quad U = U_2 \qquad -\delta_1 < y < 0, \quad U = U_1\Phi_1(y) \ .$$

Let $\delta_1/\delta_2 = \omega$. Then, with $\xi = 0$ as the initial point, the initial and boundary conditions for the solution of Equation 10 are

$$\begin{aligned} \Phi(o,\zeta) &= \lambda \ ; \ -\infty < \zeta < -\omega \ ; \\ \Phi(0,\zeta) &= \Phi_1(\zeta) \ ; \ -\omega < \zeta < 0 \ ; \\ \Phi(0,\zeta) &= \Phi_2(\zeta) \ ; \ 0 < \zeta < 1 \ ; \\ \Phi(0,\zeta) &= 1 \ ; \ 1 < \zeta < \infty \ ; \text{ and} \\ \Phi(\xi, -\infty) &= \lambda \\ \Phi(\xi, +\infty) &= 1 \end{aligned} \Big\} \ \xi > 0 \ . \qquad (11)$$

Letting $\eta = \dfrac{\zeta}{2\sqrt{\xi}}$, $\eta_2 = \dfrac{1}{2\sqrt{\xi}}$, and $\eta_1 = \dfrac{-\omega}{2\sqrt{\zeta}}$ we have

$$\eta - \eta_2 = \frac{\zeta - 1}{2\sqrt{\xi}} \quad \text{and} \quad \eta - \eta_1 = \frac{\zeta + \omega}{2\sqrt{\xi}} \ .$$

The solution of Equation 10 satisfying the boundary conditions in Equations 11 is

$$\Phi(\eta; \Phi_1, \Phi_2, \eta_1, \eta_2) = \frac{1}{2}\left[1 + \operatorname{erf}(\eta - \eta_2)\right] + \frac{1}{\sqrt{\pi}} \int_{\eta - \eta_2}^{\eta} \Phi_2 \left(\frac{\eta - \beta}{\eta_2}\right) e^{-\beta^2} \, d\beta$$

$$+ \frac{\lambda}{2}\left[1 - \operatorname{erf}(\eta - \eta_2)\right] - \frac{\lambda}{\sqrt{\pi}} \int_{\eta - \eta_1}^{\eta} \Phi_1 \left(\frac{\eta - \beta}{\eta_1}\right) e^{-\beta^2} \, d\beta \ , \qquad (12)$$

where

$$\operatorname{erf}(z) = \frac{2}{\sqrt{\pi}} \int_0^z e^{-\beta^2} \, d\beta \ .$$

$\Phi_1(\zeta)$ and $\Phi_2(\zeta)$ are the measured initial velocity distributions, and η_1 and η_2 are functions of x, c, and $f(\psi)$. The quantities c and $f(\psi)$ must be determined from experiment.

Equation 12 is a solution of Equation 6 satisfying the boundary conditions in Equations 11. It is also a solution of Equation 4 with a redefinition of Φ_1 and Φ_2 in terms of U^2 instead of U. Only experiment can determine which, if either, describes the mixing process for two parallel supersonic flows with initial boundary layers.

In order to investigate temperature fluctuations, we may write the energy equation in the form (page 612 of Reference 10)

$$\frac{D}{Dt}\left(C_pT_1 + \frac{u^2}{2}\right) - \frac{1}{\rho}\frac{\partial p}{\partial t} = \frac{k}{\rho C_p}\frac{\partial^2}{\partial y^2}\left(C_pT_1 + \sigma\frac{u^2}{2}\right) \ , \qquad (13)$$

where T_1 is the ambient temperature, σ is the Prandtl number ($\sigma = C_p \mu/k$), and

$$\frac{D}{Dt} = \frac{\partial}{\partial t} + u\frac{\partial}{\partial x} + v\frac{\partial}{\partial y} \quad .$$

As in Equation 1 we neglect pressure fluctuations and we set

$$u = U + u', \quad v = V + v', \quad T_1 = T + T', \quad \text{and} \quad \rho = \frac{p}{RT} \quad . \tag{14}$$

We substitute these relations in Equation 13 and take mean values. Then,

$$U\frac{\partial}{\partial x}\left(C_pT + \frac{U^2}{2} + \overline{\frac{u'^2}{2}}\right) + \overline{u'\frac{\partial}{\partial x}(C_pT' + Uu')}$$

$$V\frac{\partial}{\partial y}\left(C_pT + \frac{U^2}{2} + \overline{\frac{u'^2}{2}}\right) + \overline{v'\frac{\partial}{\partial y}(C_pT' + Uu')} =$$

$$\overline{\frac{kR}{C_{pp}}(T + T')\frac{\partial^2}{\partial y^2}\left[C_p(T + T') + \sigma\frac{U^2}{2} + \sigma Uu' + \sigma\frac{u'^2}{2}\right]} \quad .$$

If we assume that the incompressible continuity equation is approximately valid, the expression

$$C_p\left[\frac{\partial u'}{\partial x} + \frac{\partial v'}{\partial y}\right]T' + \left[\frac{\partial u'}{\partial x} + \frac{\partial v'}{\partial y}\right]Uu' = 0$$

is added to the left side and T' is neglected in the numerator in the right, then the equation becomes

$$\left[U\frac{\partial}{\partial x} + V\frac{\partial}{\partial y}\right]\left[C_pT + \frac{U^2}{2} + \overline{\frac{u'^2}{2}}\right] + C_p\frac{\partial}{\partial x}\overline{u'T'} + C_p\frac{\partial}{\partial y}\overline{v'T'}$$

$$+ \frac{\partial}{\partial x}\left(\overline{Uu'^2}\right) + \frac{\partial}{\partial y}\left(\overline{Uu'v'}\right) = \frac{k}{\rho C_p}\frac{\partial^2}{\partial y^2}\left[C_pT + \sigma\frac{U^2}{2} + \sigma\overline{\frac{u'^2}{2}}\right] . \tag{15}$$

In this equation we neglect $\overline{u'^2}$ compared with U^2,

$$C_p\frac{\partial}{\partial x}\overline{u'T'} \text{ and } C_p\frac{\partial}{\partial x}\left(\overline{Uu'^2}\right)$$

compared with the other two turbulent transfer terms, and $V\frac{\partial}{\partial y}(\ )$ compared with $U\frac{\partial}{\partial x}(\ )$. Further, we set

$$\overline{v'T'} = -\frac{k_t}{\rho C_p}\frac{\partial T}{\partial y}$$

$$\overline{u'v'} = -\frac{\epsilon}{\rho}\frac{\partial U}{\partial y} \quad . \tag{16}$$

Then Equation 15 becomes

$$U \frac{\partial}{\partial x}\left(C_pT + \frac{U^2}{2}\right) = \frac{k}{\rho C_p}\frac{\partial^2}{\partial y^2}\left(C_pT + \sigma\frac{U^2}{2}\right) + \frac{k_t}{\rho C_p}\frac{\partial^2}{\partial y^2}\left(C_pT + \frac{C_p\epsilon}{k_t}U^2\right).$$

If we write the turbulent Prandtl number $\sigma_t = C_p\epsilon/k_t$ and neglect laminar transfer compared with turbulent, we get

$$U \frac{\partial}{\partial x}\left(C_pT + \frac{U^2}{2}\right) = \frac{k_t}{\rho C_p}\frac{\partial^2}{\partial y^2}\left(C_pT + \sigma_t\frac{U^2}{2}\right). \tag{17}$$

Now let $\sigma_t = 1$, $U = (U_1+U_2)/2$, and write $C_pT_o = C_pT + U^2/2$, where T_o is the stagnation temperature. Then

$$\frac{\partial T_o}{\partial x} = \frac{2k_t}{\rho C_p U_2(\lambda + 1)}\frac{\partial^2 T_o}{\partial y^2}. \tag{18}$$

This equation is identical in form with Equation 6. Further, the boundary conditions on T_o are given by Equation 11 with only a change in the symbols. Hence, within the framework of the above simplifications, Equation 12 describes the spreading of the stagnation temperature as well as of the momentum.

The integrals appearing in Equation 12 were evaluated numerically for increments of $\eta_2 = 1.0$ in the range of $0 < \eta_2 < 10$ and for increments of $\eta = .5$ in the range $-3.0 < \eta < \eta_2 + 3.0$. The values of Φ_1 and Φ_2 were given by the experimental results described in Section V. These functions were taken as $\Phi_1 = (y/\delta_1)^{1/7}$, $\Phi_2 = (y/\delta_2)^{1/5}$. The results of the computations are presented graphically in Figure 2.

III. DESCRIPTION OF EXPERIMENTAL EQUIPMENT

The mixing phenomena were studied in the region downstream of the lip at which the two supersonic streams merge. The supersonic streams were generated by means of a double-corner nozzle as shown in Figure 3. Figure 4 is a photograph of the setup with one side of the lower settling chamber removed, showing a side view of the honeycomb used in the lower set. Figure 5 shows the two channels with one of the tunnel side plates removed.

The double channel is 4 inches wide and the vertical dimensions of the upper and lower streams are, respectively, 4 and 2 inches. The coordinates of the contoured steel nozzle blocks are those obtained from Reference 14, and permit a variation of Mach number in each channel of from 1.4 to 4.0 by translation of the lower block of each channel with respect to the upper block.

In order to insure sufficient strength in the tip of the cantilevered middle nozzle block, it was necessary to rotate the lower contour of the middle nozzle block 1°. This causes the secondary jet to impinge on the main jet at an angle of 1°. This inclination is in addition to that prescribed by the rate of boundary-layer growth, which amounts to about 1.5°. The total angle between upper and lower surface is therefore 2.5°. Since both streams are supersonic, the small degree of nonparallelism of the main stream will be adjusted by the shocks and expansions at the lip. Details of the construction are given in Appendix A.

All the total pressures were measured with a .043-inch-diameter stainless-steel pitot probe attached to a mercury manometer. The accuracy of these measurements is ± .03-inch Hg. The height of the probe with respect to the lip on the middle nozzle block was measured with a cathetometer by viewing the probe through the glass window before each run. The amount of probe deflection was checked by measuring this dimension during a run. The deflections were generally within the reading error of the cathetometer, which is ± .01 centimeter.

The total pressure in the settling chamber was measured with a mercury manometer which read the static wall pressure in a region where the velocity was essentially zero. The total pressure in the primary jet was the atmospheric pressure recorded on a standard barometer.

For the pressurized operation, the stagnation pressure of the upper jet, which was approximately 60 pounds per square inch absolute, and the total pressure at the pitot probe were measured with 100-inch U-tube mercury manometers, while the stagnation pressure in the lower jet was measured with a 30-inch single-tube mercury manometer. The reading errors for these runs were ± .5-inch Hg since the throttling valves were manually operated.

The total temperature profiles were measured with a shielded thermocouple probe similar to the probe which is described in detail in Reference 11. The thermocouple was attached to a sensitive galvanometer in a Consolidated Recorder. The reading accuracy of this system is ± 0.1°F. The total temperature in the settling chamber of the upper jet was measured at first with a simple dial-type thermometer, and later when it became apparent that this method was not sufficiently accurate, an unshielded standard thermocouple was mounted in the duct upstream of the entrance to the main or upper jet. The output of this thermocouple was again used to deflect a galvanometer of the Consolidated Recorder.

IV. EXPERIMENTAL RUNS

Total pressure profiles in the mixing region were measured at several stations downstream of the lip for the following ratios of Mach number and jet to stream static pressure: (1) $M_1 = 1.9$, $M_2 = 2.5$, $p_2/p_1 = 1$; (2) $M_1 = 1.9$, $M_2 = 3.2$, $p_2/p_1 = 1$ and .25; (3) $M_1 = 0$, $M_2 = 2.5$. Additional total pressure profiles were measured for configuration (1) with the Reynolds number increased by a factor of 4, i.e., at stagnation pressure of 60 pounds per square inch absolute. Total temperature profiles in the mixing region were measured only in cases (1) and (2-b) above.

With configuration (1) an attempt was made to alter the boundary-layer thickness in the upper or main jet by sucking a part of the boundary layer through 4-inch x .035-inch longitudinal slots in the windows. The downstream ends of the slots were 4-inches upstream of the lip (see Figure 6). This slot size was the maximum which could be used with the existing pumping capacity and still maintain critical pressure ratio across the slots. Rough computations using this slot size indicate that a maximum of approximately 15 percent of the mass flow in the floor and side-wall boundary layers can be removed through these slots.

Schlieren photographs of all configurations were taken.

V. EXPERIMENTAL RESULTS AND DISCUSSION

CONFIGURATION (1) ($M_1 = 1.9$, $M_2 = 2.5$, $p_2/p_1 = 1.0$)

The schlieren photograph in Figure 7 illustrates the flow obtained with this configuration.

It will be observed that the finite thickness of the lip, although it is only .025 inches, still results in weak shock waves at the lip in both upper and lower streams even when $p_2/p_1 = 1.0$. The most striking result of the whole flow is the extremely low angle of spread of the mixing region; it is no greater than the normal rate of growth of the original boundary layers. It is apparent that the mixing phenomenon is confined mainly to the two boundary layers.

The experimentally determined velocity profiles are compared in Figure 9 with the theoretical velocity profiles determined from Equation (12). The initial conditions are specified as $\delta_2 = .89$ centimeters, $\omega = .605$, $\lambda = .873$, $n_2 = 1/5$ and $n_1 = 1/7$, where n_2 and n_1 are the exponents used in the initial boundary-layer velocity profiles. These initial conditions were determined from velocity profiles measured at the lip (see Figure 8). The appropriate value of η_2 for each value of ψ was determined by applying the least-squares method to the experimental points and the theoretical curves. The solid curve is a solution of Equation (6) while the dashed curve is a solution of Equation (4). In an attempt to decide which Equation [(4) or (6)] better describes the physical phenomenon, the standard deviations, σ, have been computed and are listed below in Table I.

TABLE I

$\Phi = \frac{u}{u_2}$			$\Phi = \frac{u^2}{u_2^2}$		
ψ	η_2	σ	ψ	η_2	σ
2.4	3.8	28	2.4	4.0	26
5.3	3.1	13	5.3	3.2	11
8.1	2.5	25	8.1	2.7	19
25.4	1.7	20	25.4	1.7	12
30.0	1.6	24	30.0	1.6	16

From the values of σ in this table, it is apparent that no choice as to the diffusive quantity in Equation (12) can be made. Furthermore, it is highly unlikely that any power of the velocity ratio between 1 and 2 will fit the experimental data any better, since only a very small change in the shape of the curve is obtained in going between powers of 1 and 2.

It is apparent that a close correlation between theory and experiment cannot be achieved simultaneously for the spread of the mixing region and for the minimum velocity ratio.

CONFIGURATION (2a) ($M_1 = 1.9$, $M_2 = 3.2$, $p_2/p_1 = 1.0$)

The experimental velocity profiles measured at several stations are shown in Figure 10 together with the corresponding theoretical velocity profiles. Figure 11 is a schlieren photograph of this mixing configuration. The flow is in all essentials similar to the flow for configuration (1). Initial conditions used to compute the theoretical curves are shown in Figure 10.

CONFIGURATION (2b) ($M_1 = 1.9$, $M_2 = 3.2$, $p_2/p_1 = .25$)

The schlieren photograph of this flow is shown in Figure 12. It will be noted that at the lip the flow is deflected upward through an angle of 9.9°, as measured from several schlieren photographs. The theoretical angle of deflection required for matching static pressures is 9.6°. A Prandtl-Meyer expansion fan originates at the lip of the middle nozzle block and crosses the lower channel. This expansion wave is followed by the usual weak shock wave as evidenced by the light line which closes the expansion wave. The Mach number increases through this expansion from 1.9 to 2.3. A shock wave originates at the lip and crosses the upper channel. The shock-wave angle as measured from schlieren photographs is 26.7°, and the Mach number is reduced on crossing the shock from 3.2 to 2.7.

Figure 13 presents the total pressure profile measured with the total head probe at a distance 1.3 centimeters downstream of the origin of the mixing. All the shock waves and expansion waves which occur in the schlieren photograph of Figure 12 are easily identifiable on the total pressure profile.

The velocity profiles measured at the lip are very similar to those measured in the undeflected flow (configuration 2a). This rather remarkable feature is probably due to the fact that by far the greatest part of the boundary layer in both the deflected and undeflected cases is supersonic. There is thus only a very small subsonic channel through which pressure gradients from downstream might influence the flow upstream. This is confirmed by the schlieren photograph of Figure 12. The situation is qualitatively similar to the shock boundary-layer interaction problem where thick turbulent boundary layers are but slightly disturbed by even relatively strong shock waves. The flow phenomenon found here is essentially that at the trailing edge of a supersonic lifting wing.

The theoretical solution shown in Figure 14 was computed on the basis of boundary-layer profiles measured at the lip and ahead of the shock-wave system. Values of the initial conditions are shown in Figure 14. The free-stream velocities of both jets, however, were evaluated downstream of the shock-expansion system which originates at the lip. The theoretical curves in this case were chosen for the best mean square fit over the entire length of the curve. While the qualitative shapes of the theoretical curves agree well with the experimental, there is consistent difference between them which can only result from the radical simplifications in the theory.

CONFIGURATION (3) ($M_1 = 0$, $M_2 = 2.5$)

The schlieren photograph of this flow is shown in Figure 15. The lower jet was sealed off with a block of wood in such a way that no air could leak through. The flow deflects 10° downward through a Prandtl-Meyer expansion fan. The Mach number of

the flow increases from 2.5 to 3.0. There is a weak closing shock which follows the expansion. If one is to judge from Figure 15, it appears that the boundary-layer thickness is much reduced by passage through the expansion. The velocity measurements in Figure 16 indicate that this thinning of the boundary layer is illusory.

The theoretical solution was computed on the basis of initial conditions ahead of the expansion system. The profiles measured immediately downstream of the lip are naturally greatly distorted by the expansion wave. The theoretical curves of Figure 16 were chosen so that the slopes at the inflection point of theoretical and experimental curves match. The agreement between the curves is much better than that for the "two-stream" configurations in the previous figures. However, it is also true that for these curves the agreement between theory and experiment is less sensitive to the choice of η_2 than for the case of two-stream mixing.

Figure 17 is a plot of η_2 versus ψ for all the experiments performed; some points from Reference 9 are also shown for comparison. The authors of Reference 9 report good agreement between theory and experiment for subsonic single-jet mixing if the mixing coefficient ϵ [Equation (7)] is assumed to be given by

$$\epsilon = \epsilon_\infty \left(\frac{X}{\delta}\right)^n , \qquad (16)$$

With $n = 0.7$ (see curve marked n = .7 in Figure 17). The present experiments indicate that while the points for the single jet (configuration 3, Figure 16) fall near those of Reference 9 on Figure 17, those for the double jet are far different. Curves are shown for n = 0, -1, and -1.5 where agreement was forced at the point indicated. It appears that $n \cong -1.0$ best fits the data for $M_1 = 1.9$, $M_2 = 2.5$.

The large differences between the data given here and that of Reference 9 is probably attributable to the fact that the mixing of the two boundary layers appears to dominate the present experiments. On the other hand, for the experiments of Reference 9, the presence of the boundary layer is a secondary influence compared with the mixing of the two streams.

The stagnation-temperature profiles shown in Figure 18 for configuration (1) ($M_1 = 1.9$, $M_2 = 2.5$, $p_2/p_1 = 1.0$) indicate a gradual equalization toward the average value with increasing distance downstream of the origin of mixing. Since the surfaces had probably not reached the recovery temperature, heat transfer to the air at the surface may be responsible for the relatively high temperature ratio at the lip. Also, since the instrument averages the stagnation temperature over 0.2 centimeter, one would not expect it to register the precise recovery value.

Since the theory of Section II assumes a Prandtl number of unity, it cannot predict the experimental values in Figure 18. An approximate method for finding the "effective Prandtl number" from measurements such as those shown is given in Reference 12. The necessary calculations have not been made.

In order to investigate the effect of Reynolds number, the stagnation pressure in the upper stream was increased from 1 to 4 atmospheres for configuration 1 ($M_1 = 1.9$, $M_2 = 2.5$, $p_2/p_1 = 1.0$). The Reynolds number per foot was thereby increased from 3.1×10^6 to 12.2×10^6. The experimental points for the two Reynolds numbers are compared in Figure 9. While small differences between the two sets of experimental points are shown, these are far from consistent. We may infer that further increases in Reynolds number would not substantially alter the results shown.

Although the original purpose of the installation of boundary-layer removal equipment, which was to obtain experimental control of the parameter ω, was not realized, it is still possible to obtain valuable information from these tests. Figure 19 shows the velocity profiles measured 25.4 boundary-layer thicknesses downstream of the origin of mixing 5.1 centimeters and 7.6 centimeters from the test-section window. Measurements were made both with and without suction. In spite of the relatively large changes in velocity profile, near the window (7.6 centimeters), the velocity profile in the center (5.1 centimeters) is relatively unchanged by the application of suction. Thus the experimental data presented here represent two-dimensional mixing flow.

VI. CONCLUSIONS

Measurements of the two-dimensional mixing of two supersonic air streams with relatively thick boundary layers are presented and compared with linearized diffusion theory. The results demonstrate the following.

1) The rate of growth of the mixing region is approximately equal to the rate of growth of the turbulent boundary layer along a wall.

2) With pressure ratios as high as 4, no region of flow separation on the low pressure side upstream of the lip was observed.

3) Measurements at Reynolds numbers different by a factor of 4 indicated no significant differences between traverses across the mixing region.

4) Measurements off the centerline and at the centerline with and without suction at the side walls indicate that the mixing phenomenon investigated here is essentially two-dimensional in terms of the mean values of the flow.

5) The linearized theory of jet mixing does not provide a satisfactory framework for correlating the results. In all other applications of the theory (e.g., References 6 and 9), the boundary layers were relatively thin, so that their presence altered only slightly the mixing of the jets. In the present results, however, as implied in 1) above, the mixing phenomenon occurs mainly between the two boundary layers. It is not known how thin the boundary layers would have to be before substantial mixing would occur between the two main streams. It seems likely that conclusion 1) applies approximately, regardless of boundary-layer thickness.

6) Measurements of the mixing of a supersonic stream with still air shows again a low mixing rate but the agreement with the linearized theory is improved over that observed for two supersonic streams.

7) The mixing coefficient ϵ shows a radically different variation with ψ than for subsonic flow (References 6 and 9). In subsonic mixing, ϵ increases with ψ, while in supersonic mixing it decreases. This behavior may be rationalized on the basis that we are dealing here essentially with the mixing of the two boundary layers. The fluctuations responsible for the Reynolds stresses will decay with ψ more rapidly than in the case of the more violent mixing of two main streams.

APPENDIX

The construction of the special channel used in these experiments involved the modification of the corner nozzle developed under Contract No. AF 33(038)-23070.[13,14] The lower contour of the center block was adapted to the existing upper contour. Both contours for the lower jet were obtained from Reference 14 by simple scaling.

The maximum stress in the middle nozzle block, assuming a uniform air load of 5 pounds per square inch, occurs 1-3/4 inches upstream of the lip and has a value of 3400 pounds per square inch. The deflection of the lip, which is .025 inch thick, is .026 inch under this load. It should be mentioned here that the load of 5 pounds per square inch is considerably larger than the actual load since, when the two nozzles are in operation, the static pressures on the upper and lower surfaces of the middle nozzle block are nearly equal, even though their ratio may be high.

The contours of both nozzle blocks were checked with a vernier height gage by measuring from a fixed, ground, flat surface. In addition, the curvature of all the contoured surfaces was checked with the curvature gage of Reference 14.

The nozzle blocks were aligned by setting the angles of the straight portions in the throat and in the test section at the values indicated in Reference 14, and at the same time setting the test-section height to the proper value. This alignment was accomplished with the vernier height gage and an inside micrometer. Each nozzle block was then pinned to its slide rails using 3/8-inch-diameter dowel pins so that no rotational motion of slide rail with respect to nozzle block was possible. In spite of these precautions, some upward motion of the bottom nozzle block was detected in the early runs so that it was necessary to add an extra brace to this nozzle block.

The settling chamber is of 3/4-inch steel plate in order to stand the higher stagnation pressures which were encountered in a later phase of the test program. The air which enters the settling chamber must pass through a 1-inch-square by 9-inch-long honeycomb which straightens out the flow prior to its entry into the secondary nozzle.

Both channels are sealed along the side walls with inflatable seals made of 1/8-inch-diameter rubber tubing. Due to structural difficulties, it is impossible to continue these inflatable seals to the very lip of the middle nozzle block, so that from the lip to a point upstream 18 inches from the lip, this nozzle block is sealed by pressing felt between the nozzle block and the window. On the first few runs some leakage was present. However, by increasing the pressure on the inflatable seals and applying vacuum wax at several points, the leakage was reduced to a point where no ill effects appear in the region of supersonic flow.

REFERENCES

1. Pai, S. J., Fluid Dynamics of Jets, D. Van Nostrand, New York, 1954.

2. Tollmien, W., Turbulent Mixing, NACA TN 1085, 1945.

3. Prandtl, L., Bermerkungen zur Theorie der freien Turbulenz." Z. A. M. M. Vol. 22. 1952. pp. 241-3.

4. Reichardt, H., "Gesetzmässigkeit der freien Turbulenz." V. D. I. Serie B. Vol. 13. 1942. Forschungsheft 414.

5. Baron, L., and Alexander, L. G., "Mixing of Coaxial Jets." Chem. Eng. Prog. Vol. 47. 1951. pp. 181-4.

6. Chapman, A. J., and Korst, H. H., "Free Jet Boundary with Consideration of Initial Boundary Layer." Proc. 2nd Nat. Cong. for Applied. Mech. Univ. of Mich. Ann Arbor. 1955.

7. Weinstein, A. S., "Diffusion of Momentum from Free and Confined Slot Jets into Moving Secondary Streams. Carneigie Inst. of Tech. Scientific Rept. No. 2.

8. Pai, S. J., "Two-Dimensional Jet Mixing of a Compressible Fluid." J. A. S. Vol. 16. 1949. pp. 463-9.

9. Horst, H. H., Page, R. H., and Childs, M. E., Compressible Two-Dimensional Jet Mixing at Constant Pressure, M. E. Tech. Note 392-1. Univ. of Ill. Urbana. 1954.

10. Goldstein, S., Ed., Modern Developments in Fluid Dynamics, Oxford Engineering Science Series, 2 vols., 1938.

11. Winkler, E. M., "Design and Calibration of Stagnation Temperatures for Use at High Supersonic Speeds and Elevated Temperatures." Journal of Applied Physics. Vol. 25. 1954. pp. 231-32.

12. Cheng, Sin-I. (This theoertical study was carried out by Prof. Cheng under this contract. It will be published elsewhere.)

13. Liepman, H. P., Murphy, J. S., and Nourse, J. H., A Physical Description of a Variable Mach Number 4 x 4 Inch Pilot Corner Nozzle." Univ. of Mich. W. T. M. 246. 1953.

14. Amick, J. L., Liepman, H. P., and Reynolds, T. H., Development of a Variable Mach Number Sliding Block Nozzle and Evaluation in the Mach Number Range 1.3 to 4.0. WADC Tech. Rept. No. 55-88. 1955.

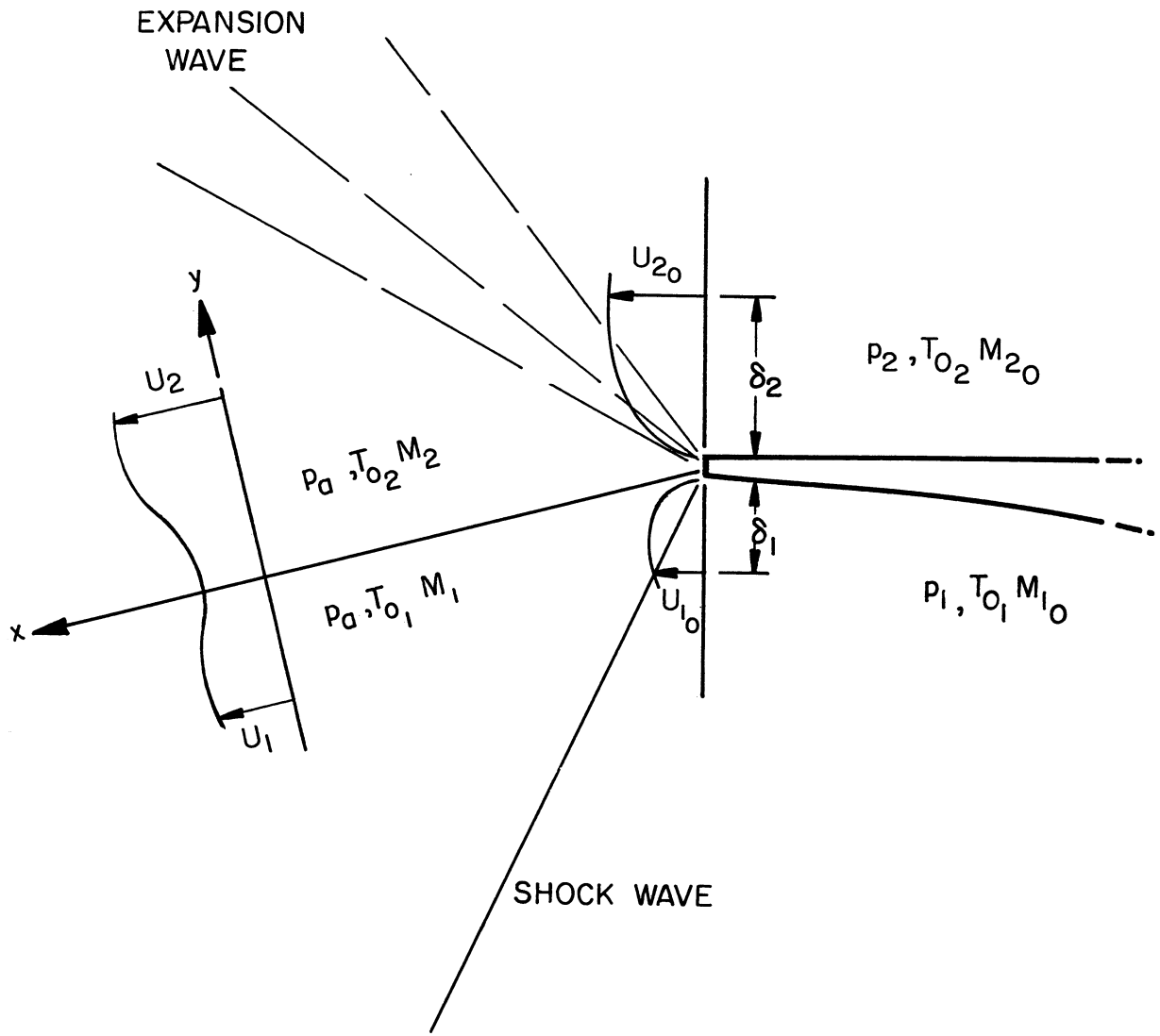

Figure 1. Diagram of mixing region.

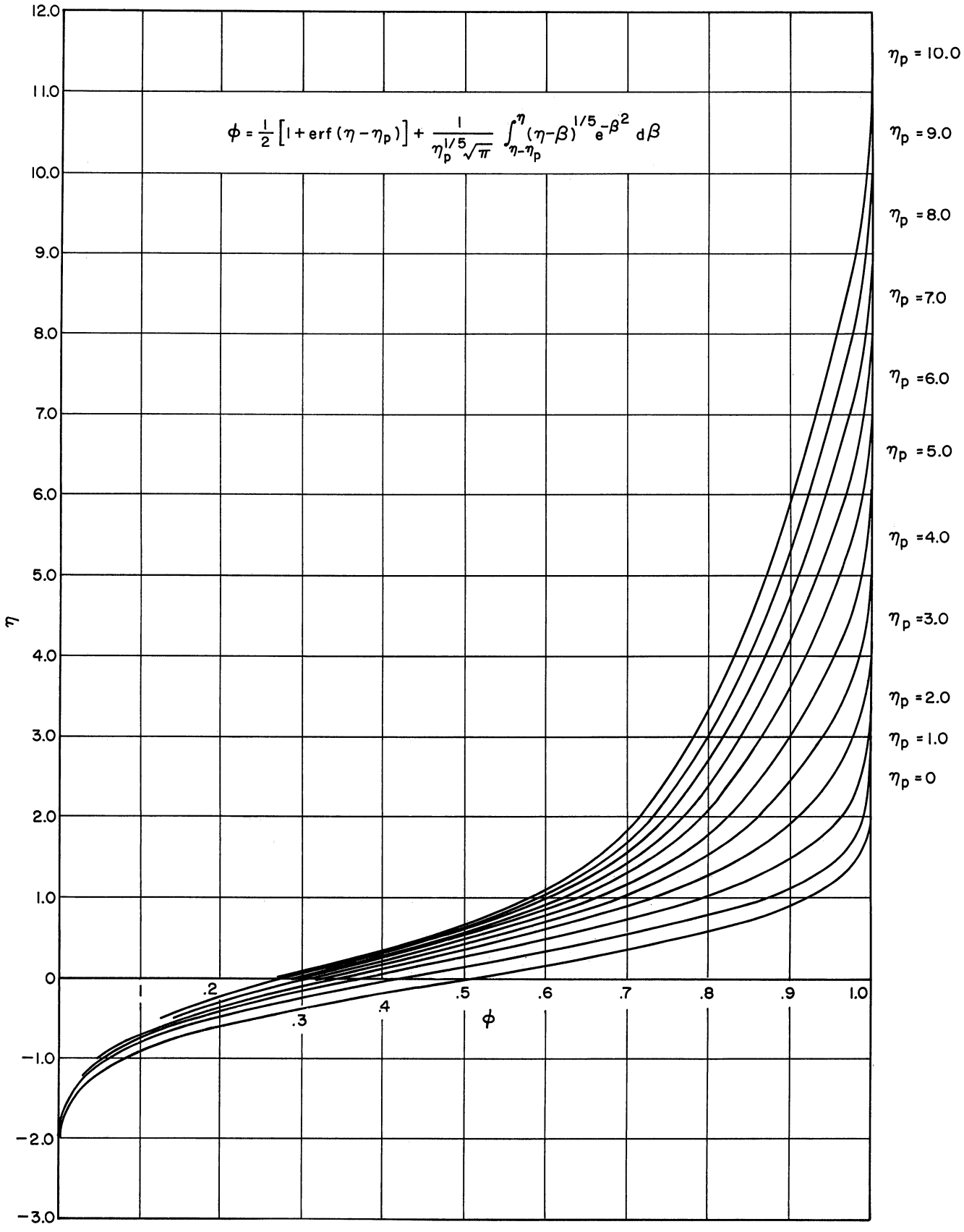

Figure 2. Theoretical velocity of profiles.

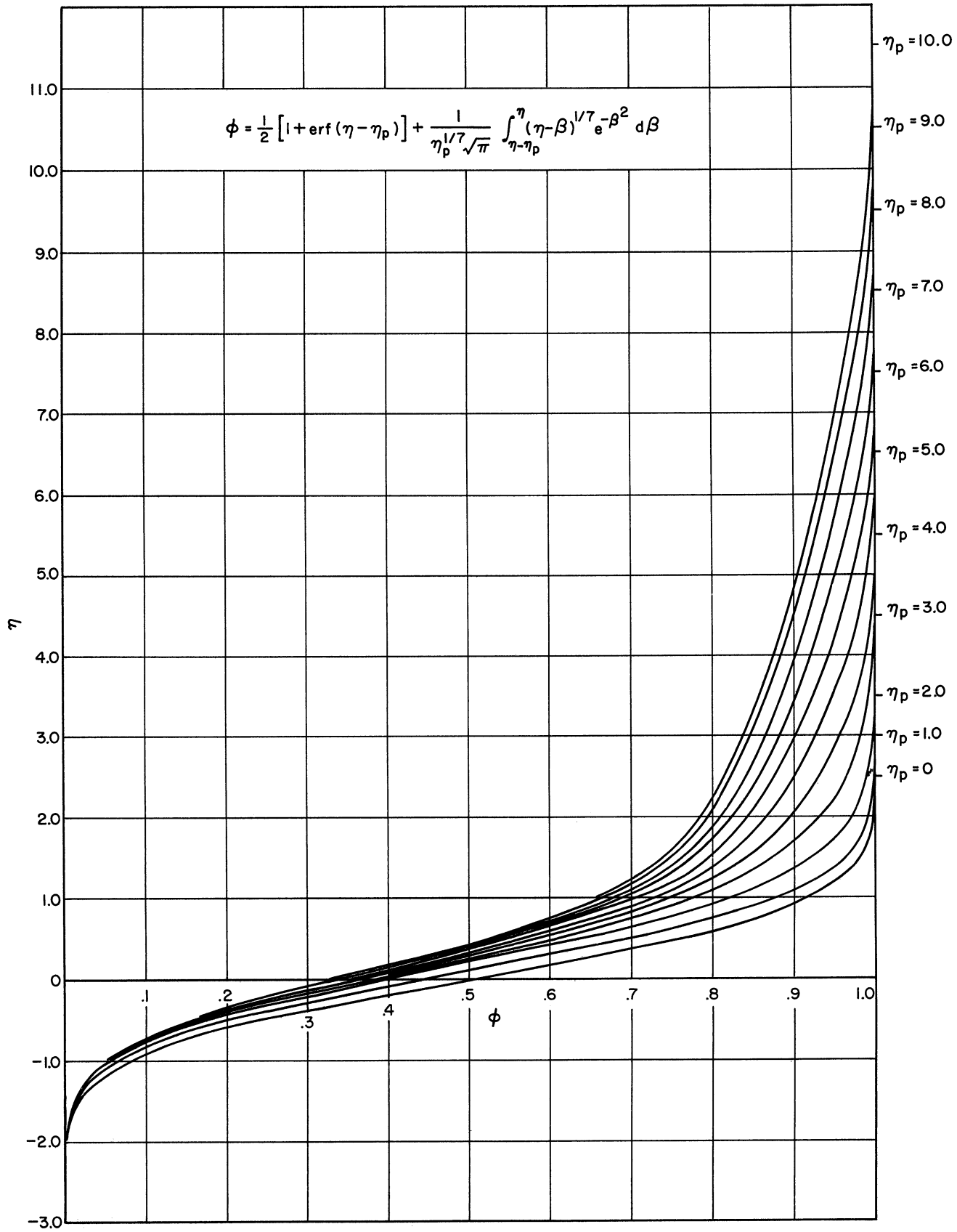

Figure 2. Concluded.

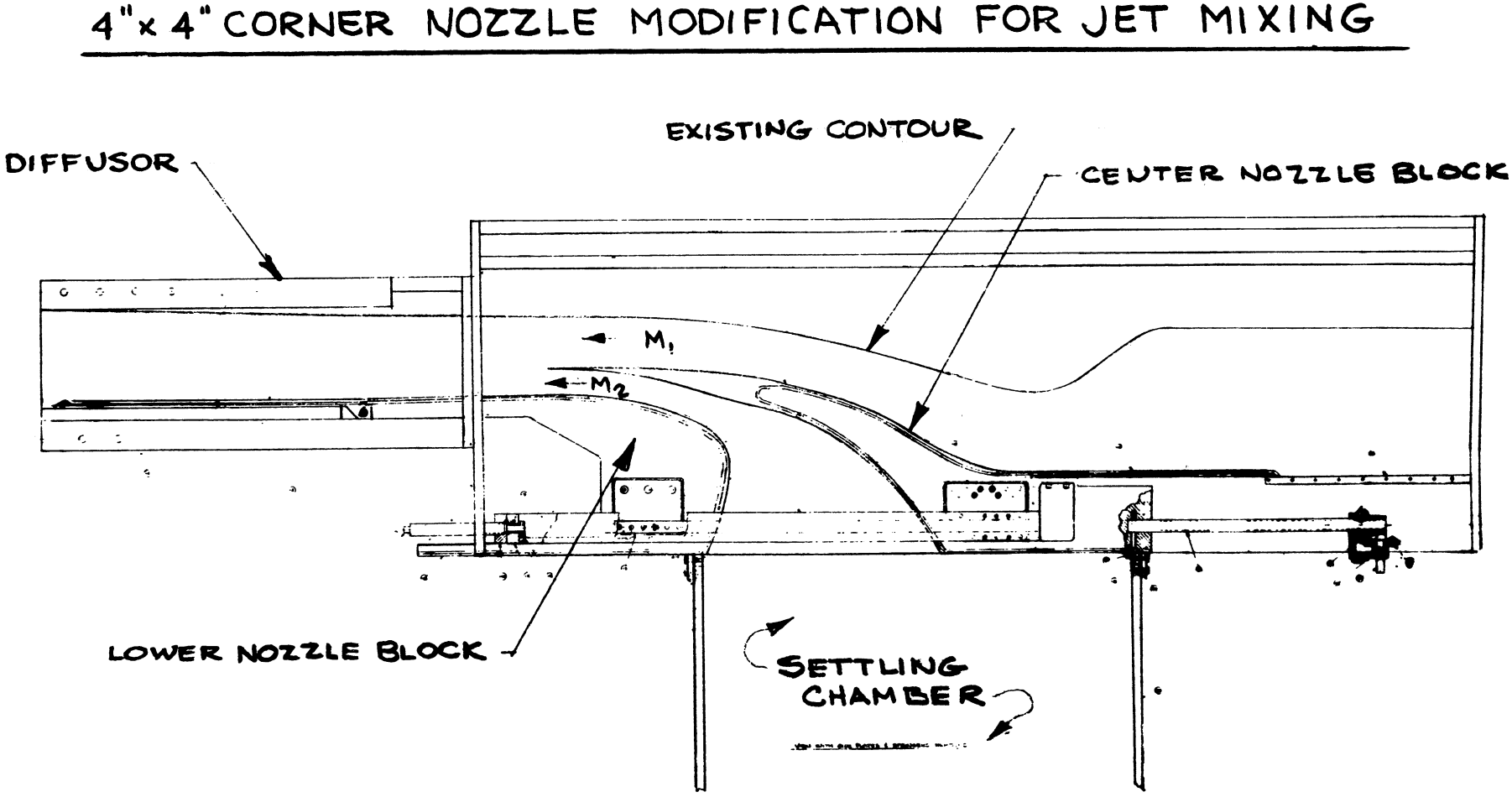

Figure 3. 4-inch by 4-inch corner nozzle modification for jet mixing

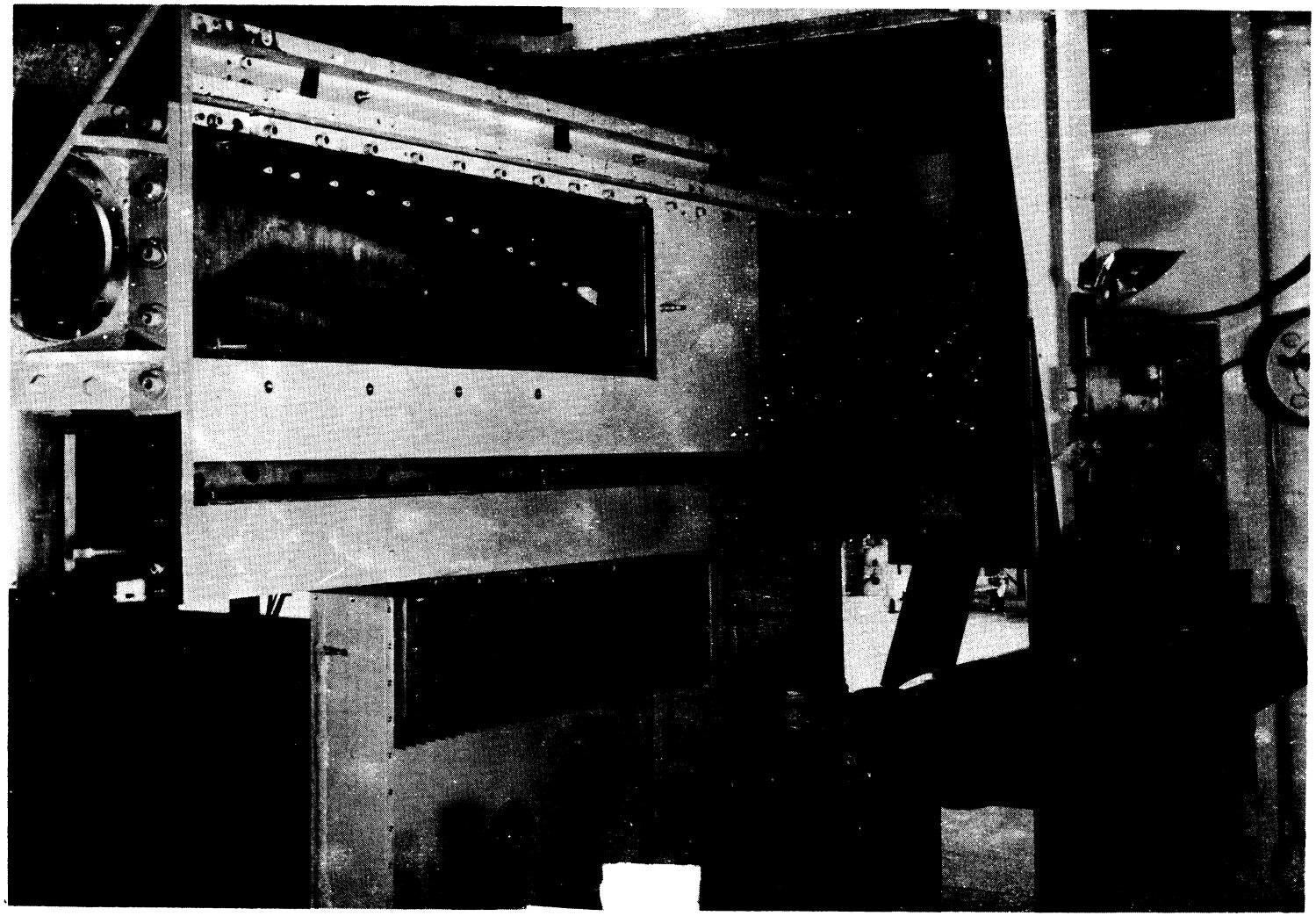

Figure 4. Sideview of the honeycomb.

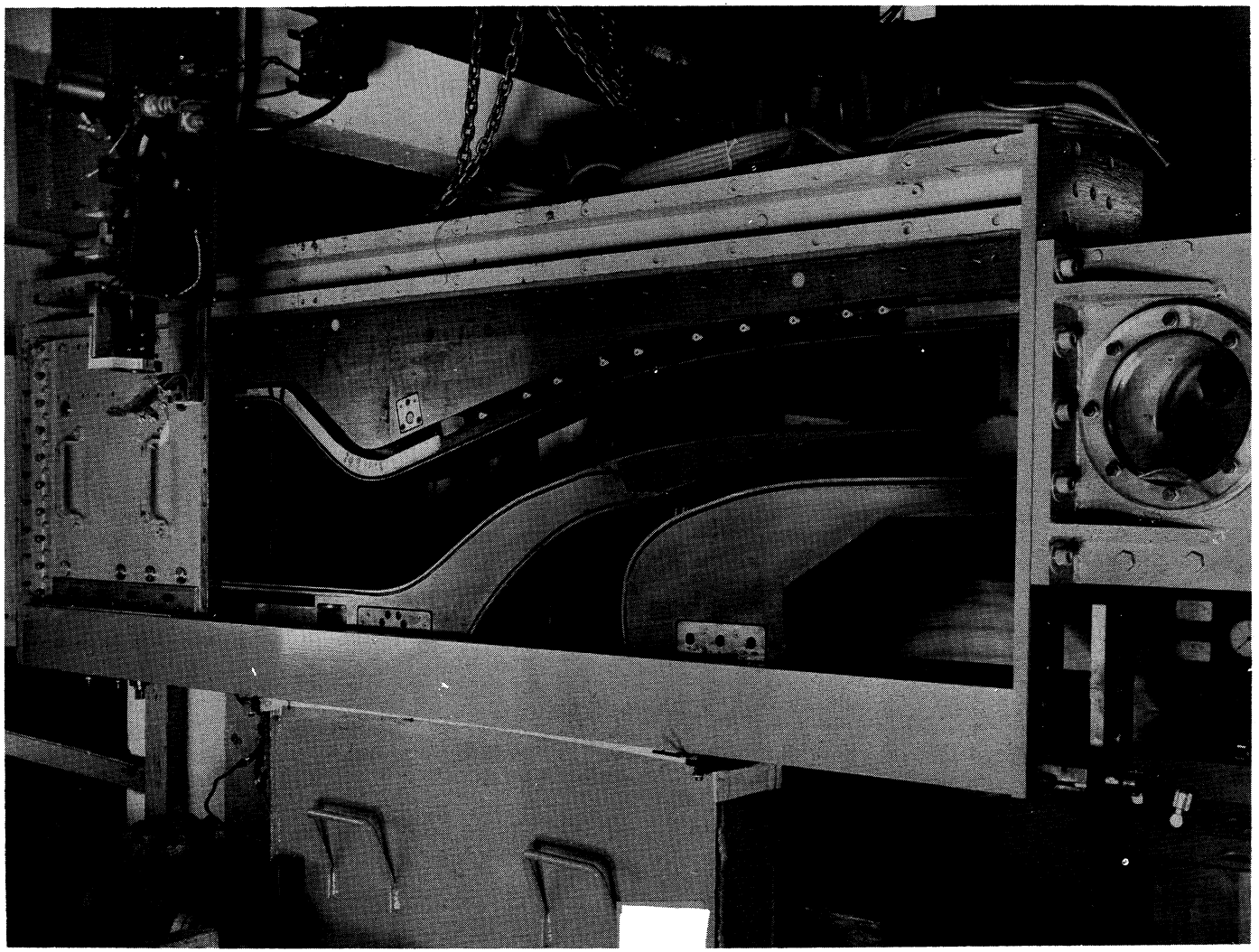

Figure 5. The two channels with one of the tunnel side plates removed.

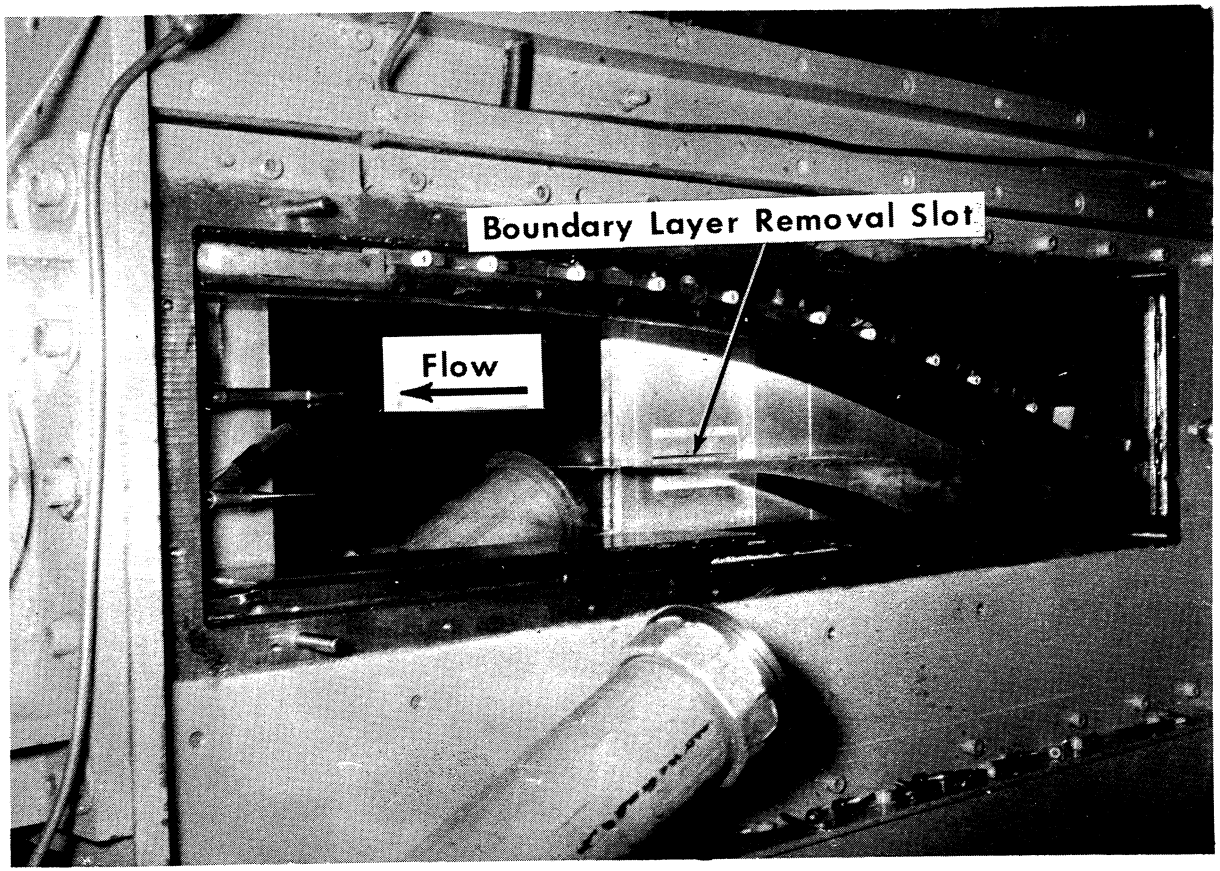

Figure 6. Boundary-layer removal equipment.

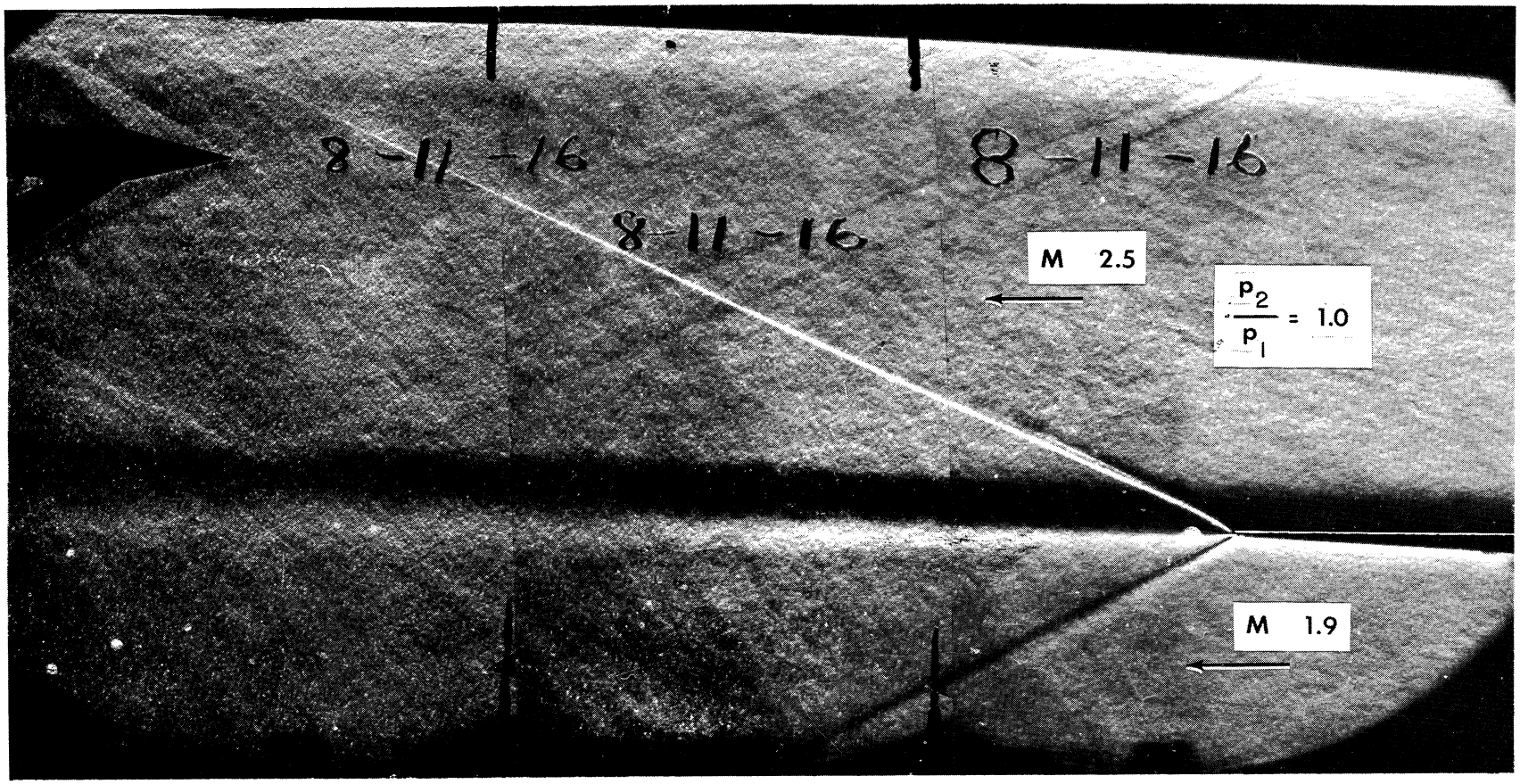

Figure 7. Schlieren photograph: $M_1 = 1.9$, $M_2 = 2.5$, $p_2/p_1 = 1.0$.

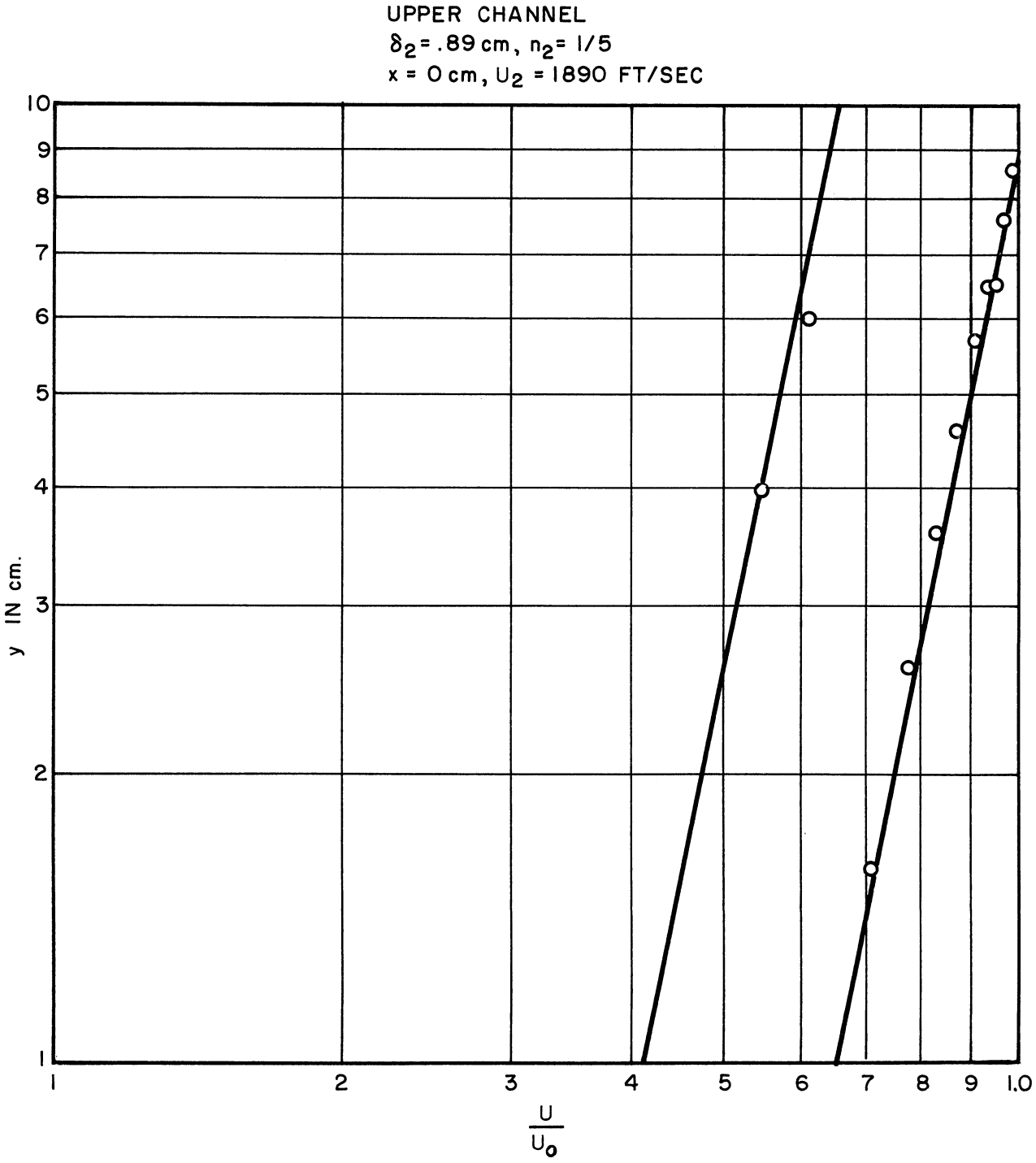

Figure 8. Initial boundary-layer profiles.

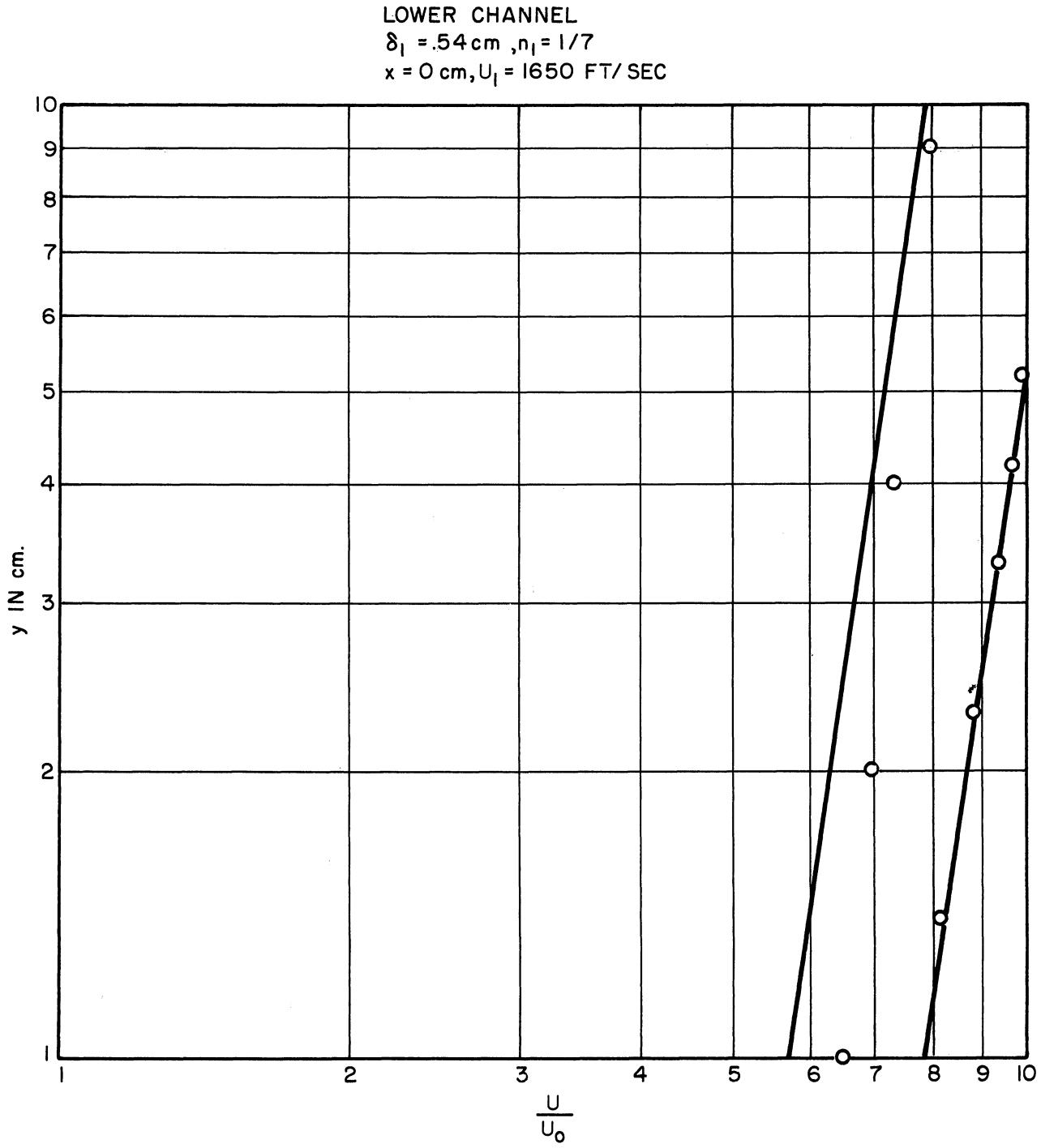

Figure 8. Concluded.

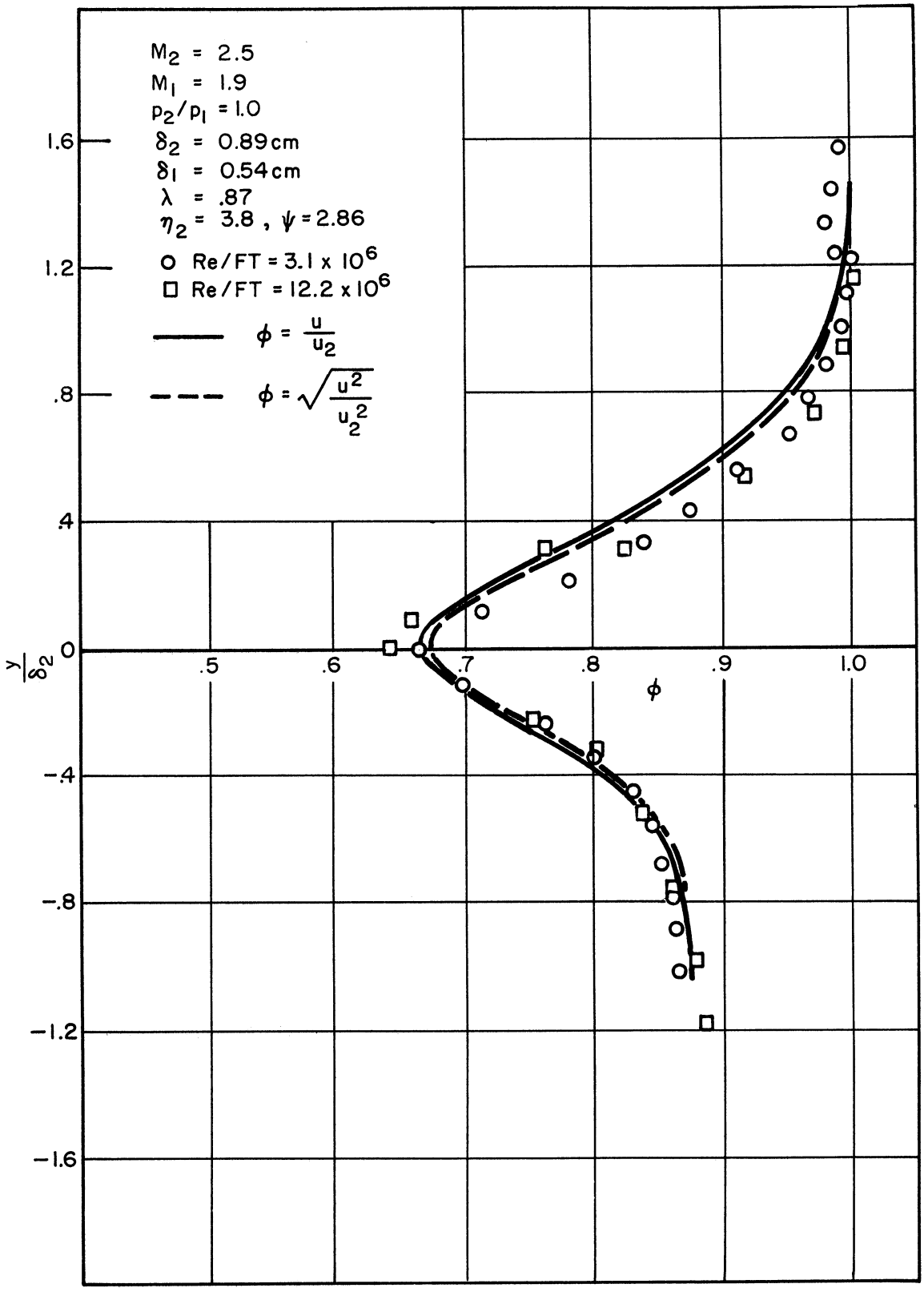

Figure 9. Theoretical and experimental velocity profiles: M_1 = 1.9, M_2 = 2.5, p_2/p_1 = 1.0.

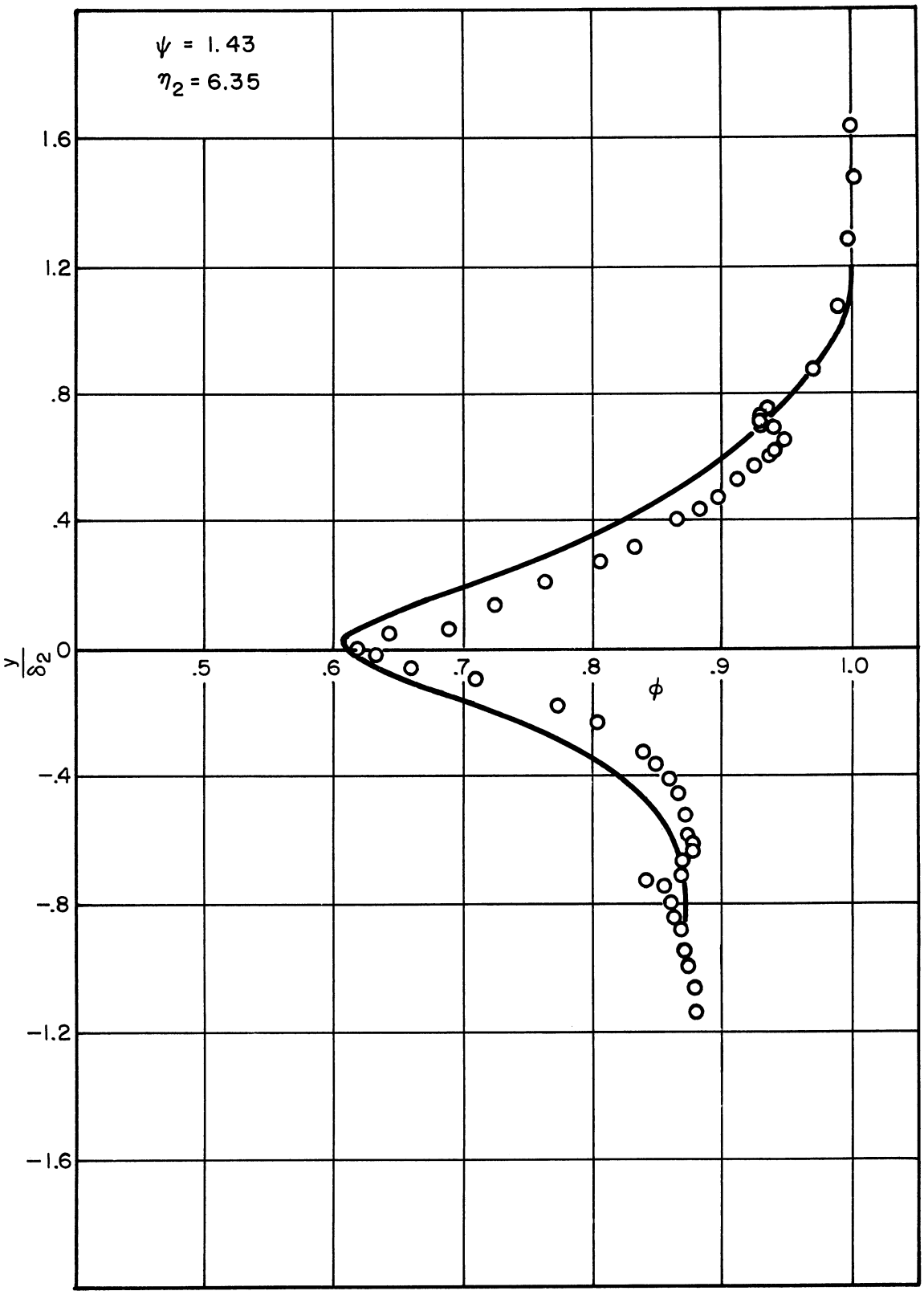

Figure 9. Continued.

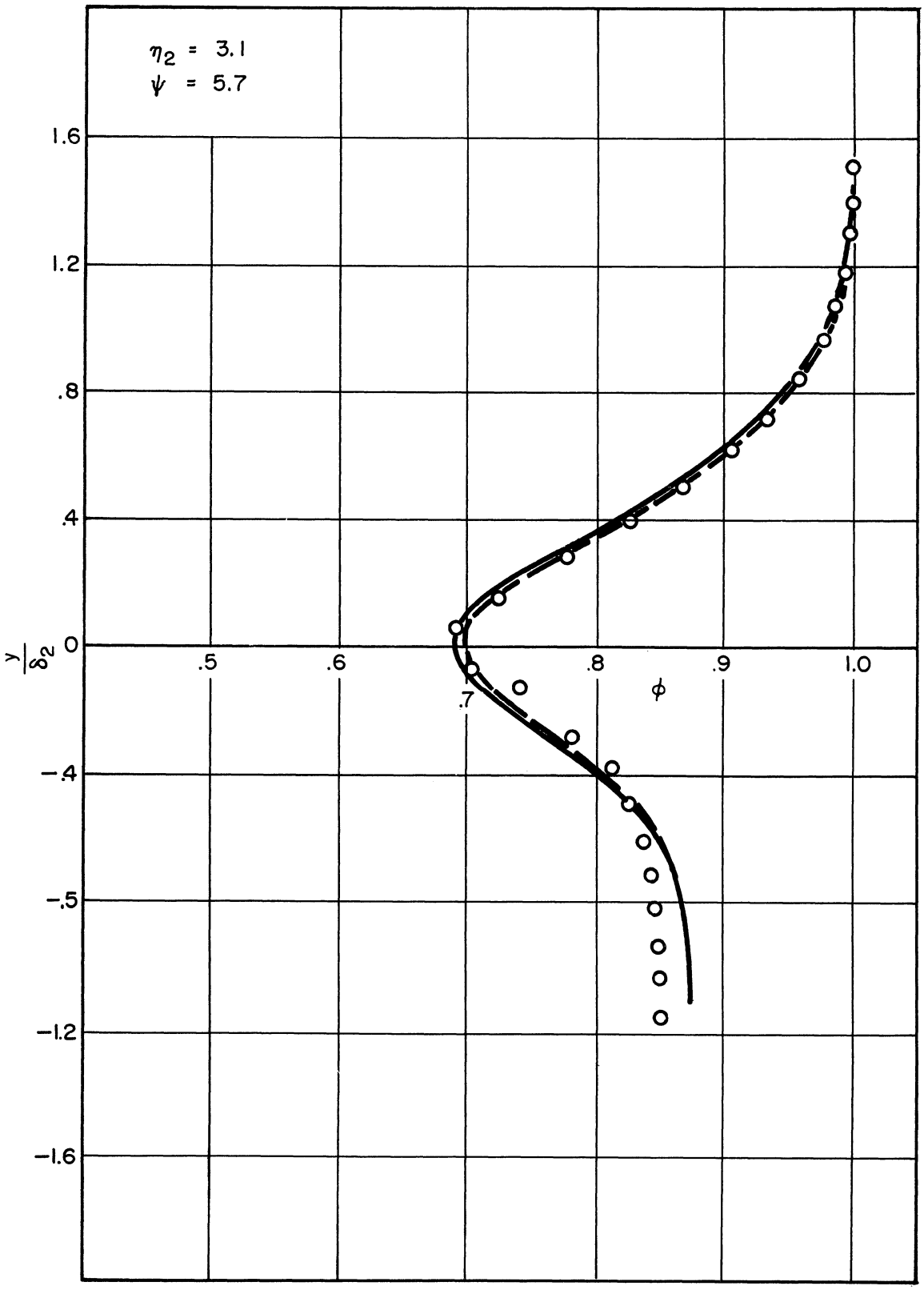

Figure 9. Continued.

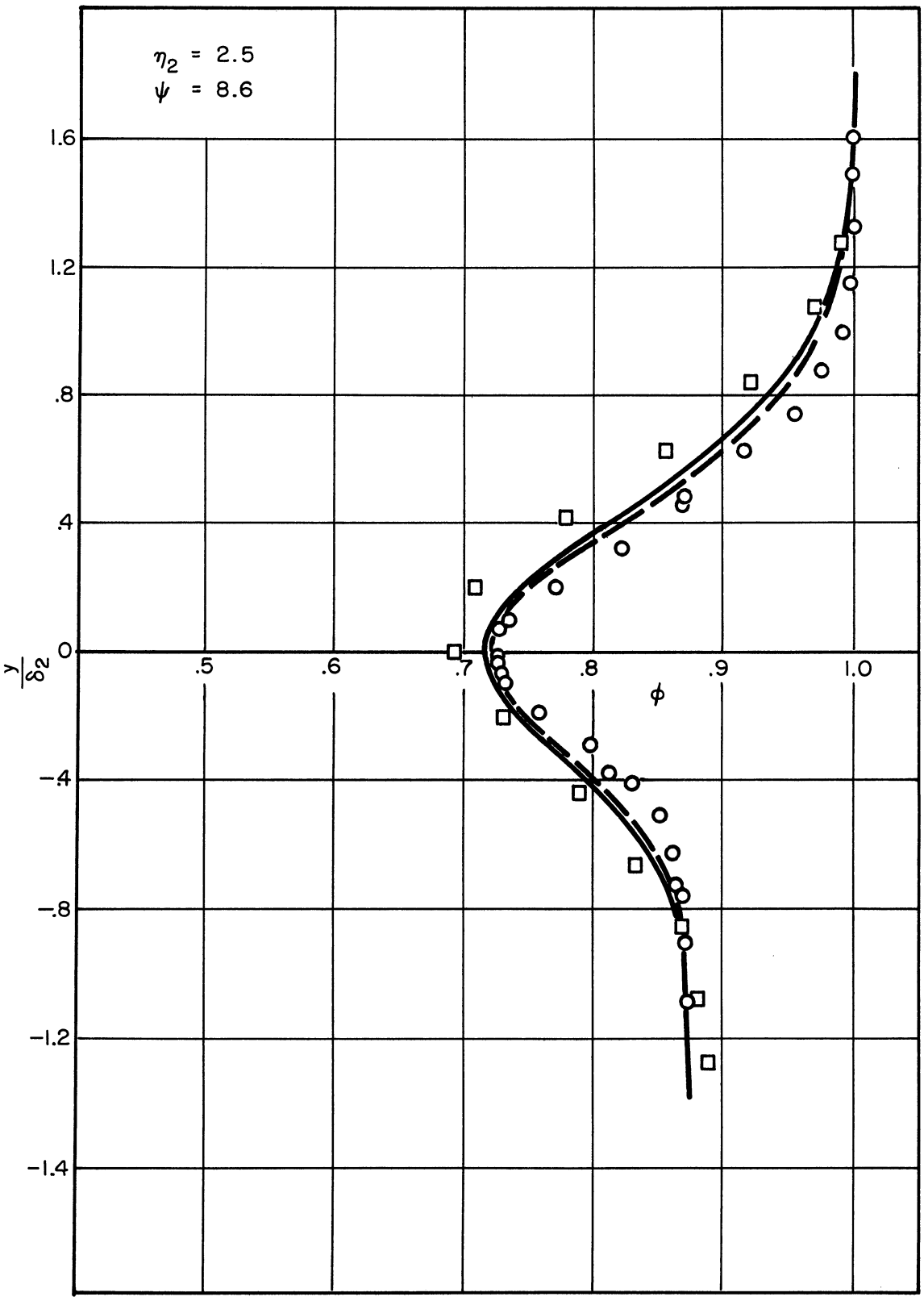

Figure 9. Continued.

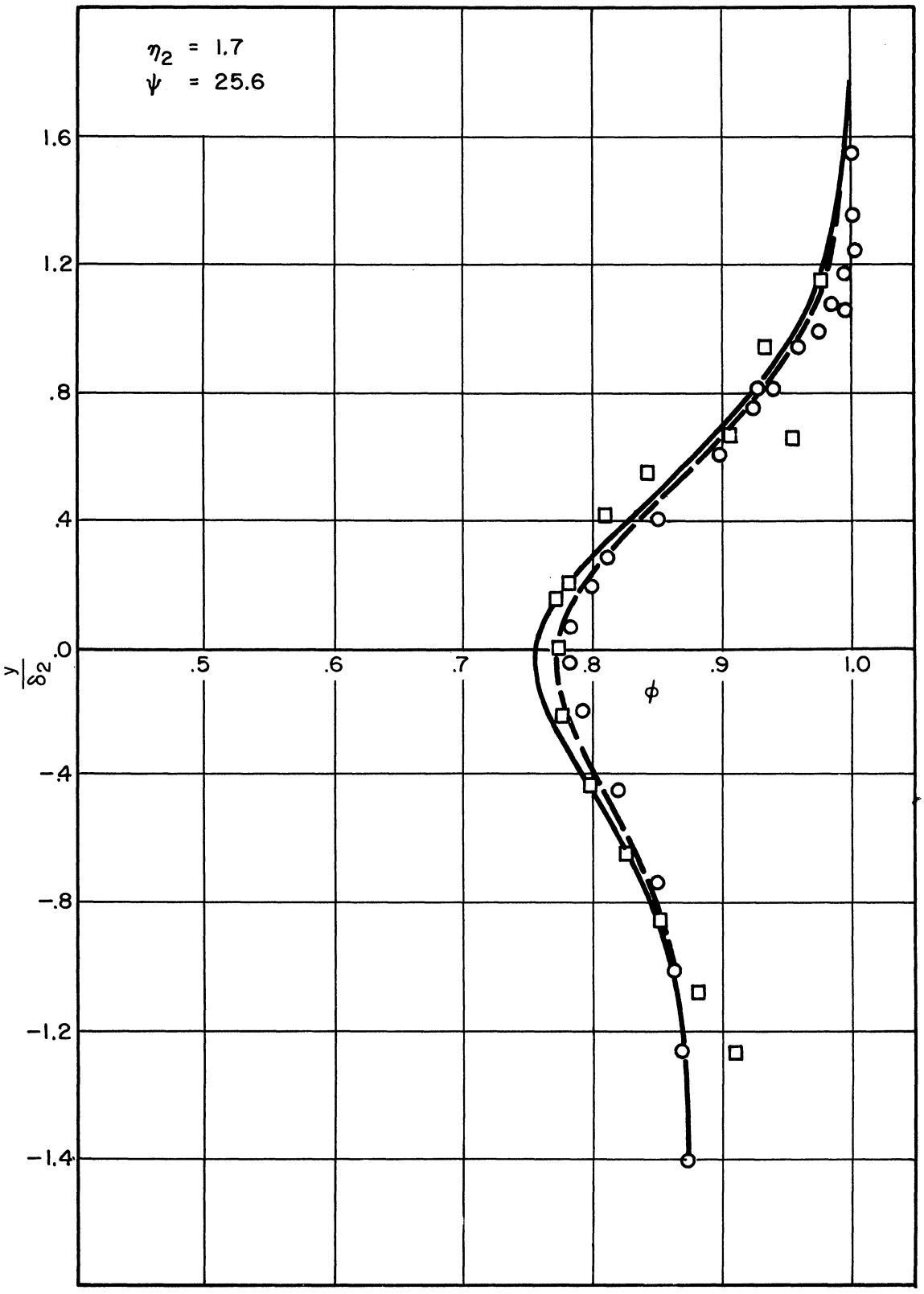

Figure 9. Continued.

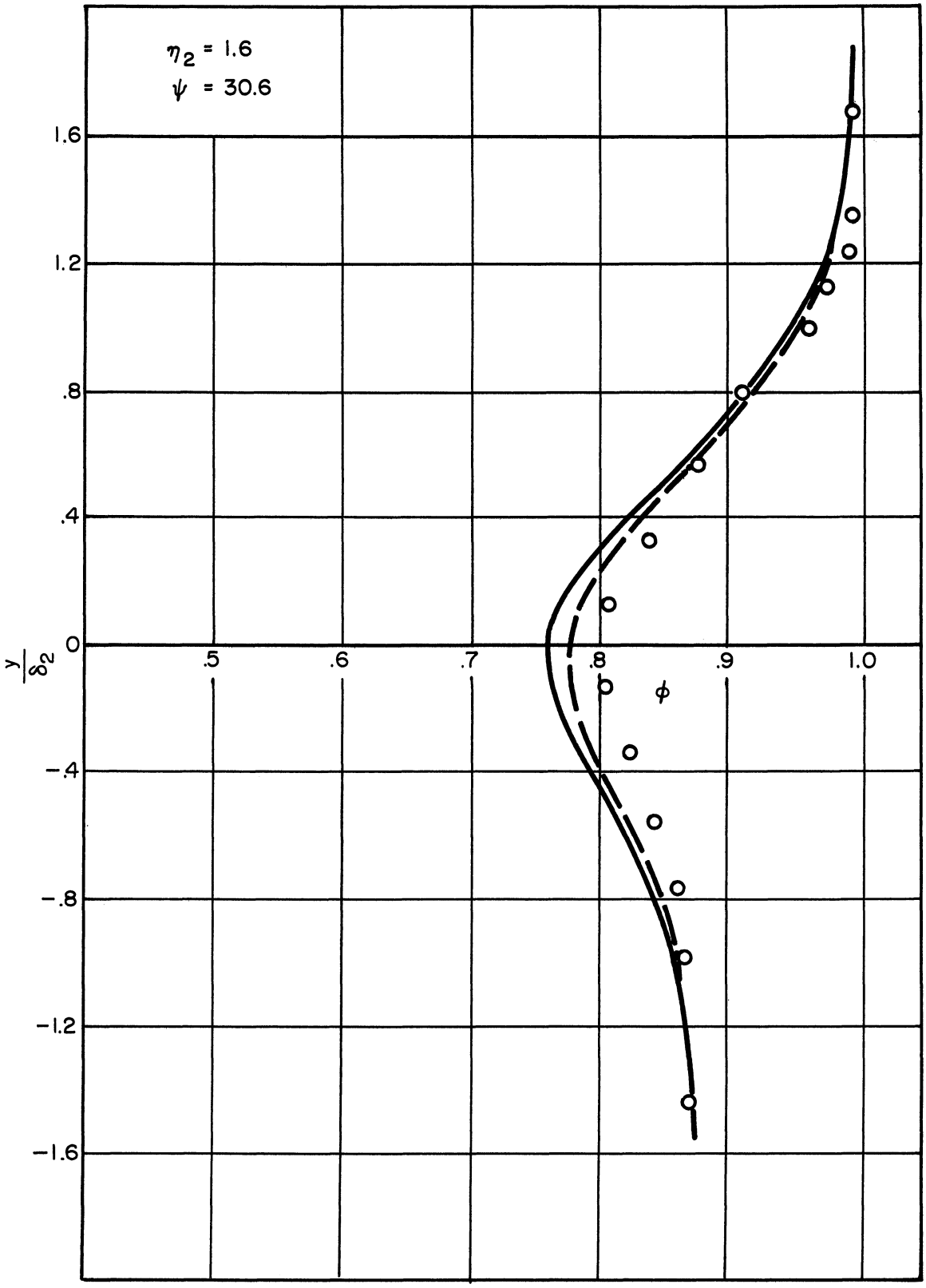

Figure 9. Concluded.

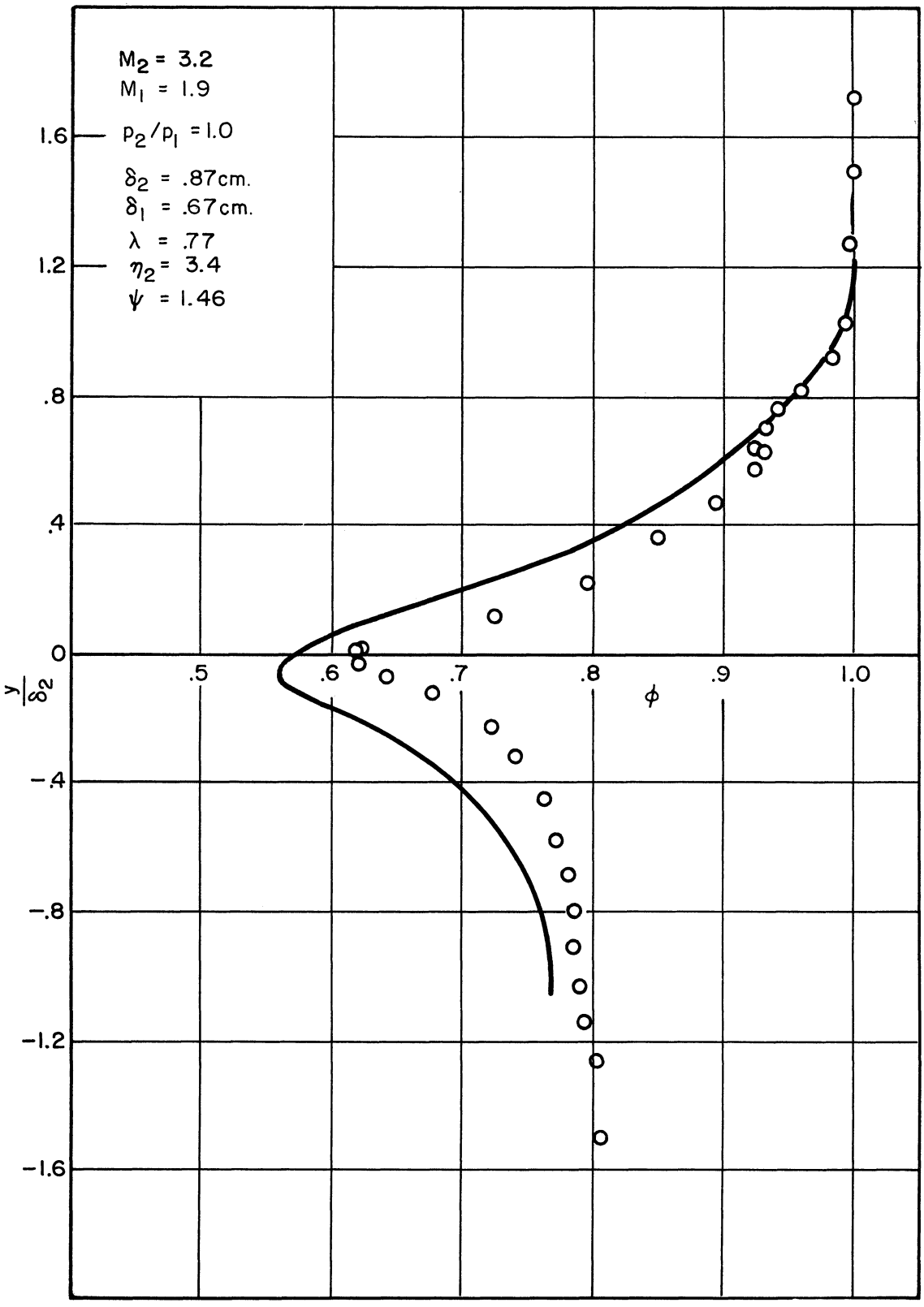

Figure 10. Theoretical and experimental velocity profiles: $M_1 = 1.9$, $M_2 = 3.2$, $p_2/p_1 = 1.0$.

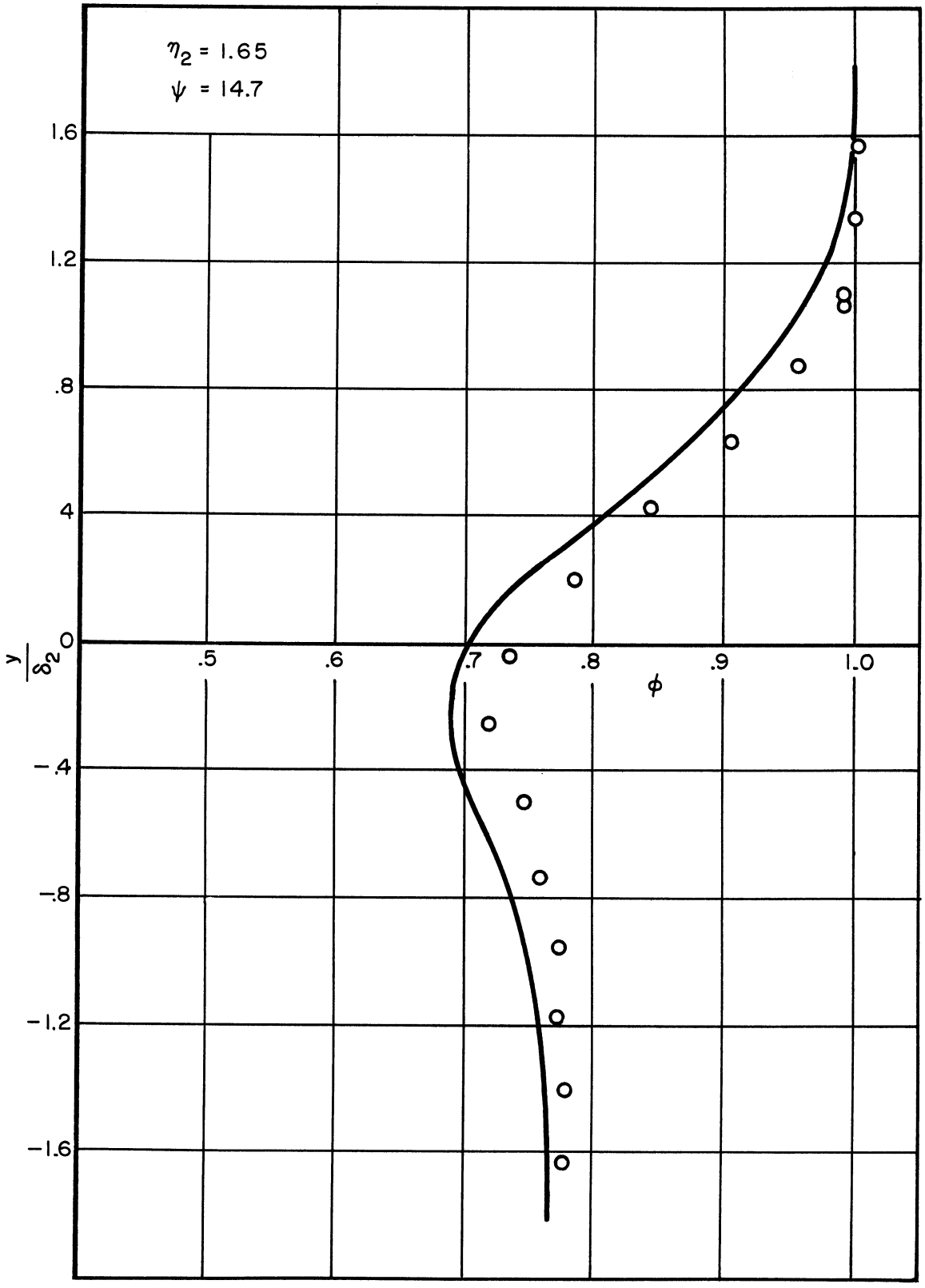

Figure 10. Continued.

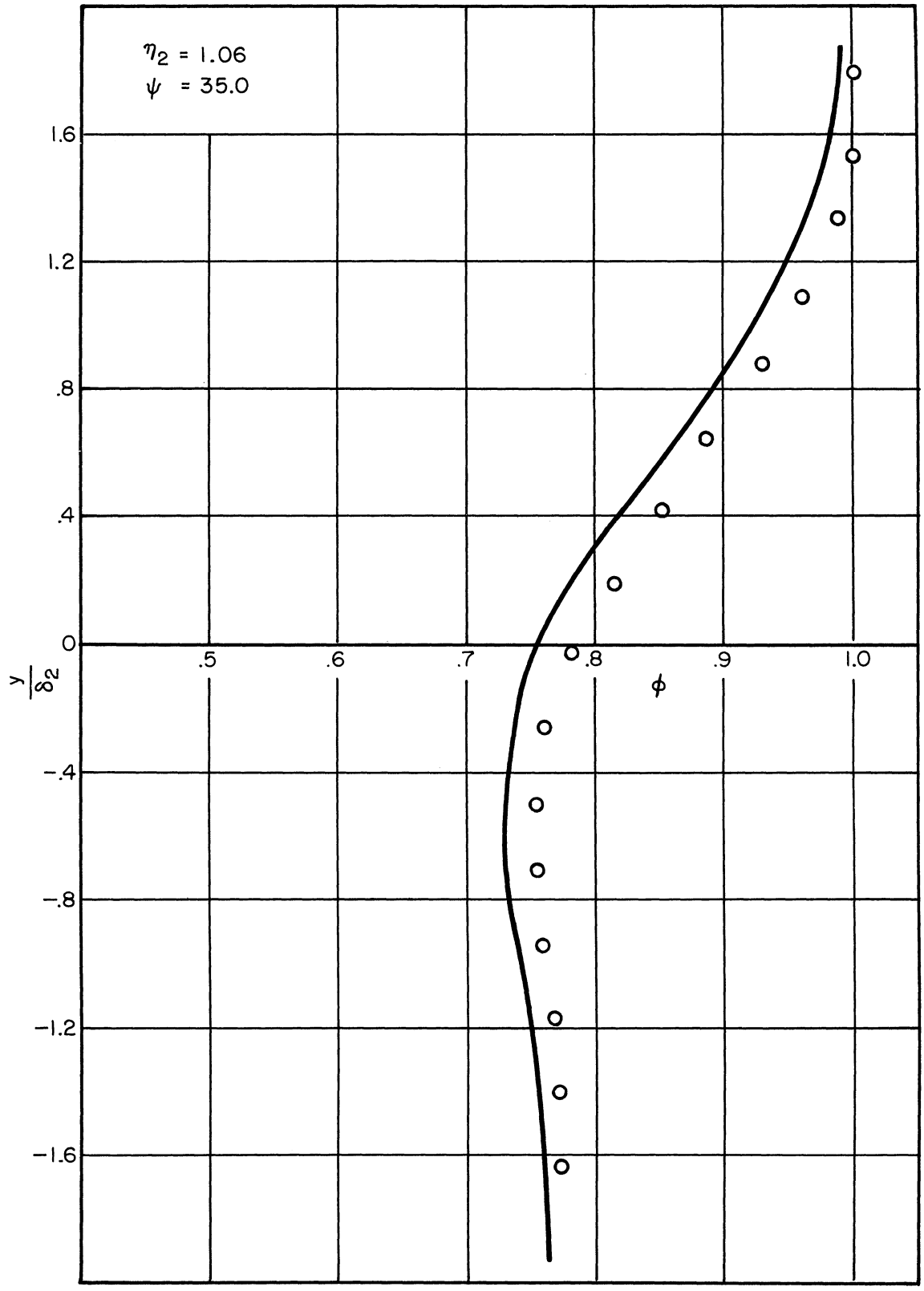

Figure 10. Concluded.

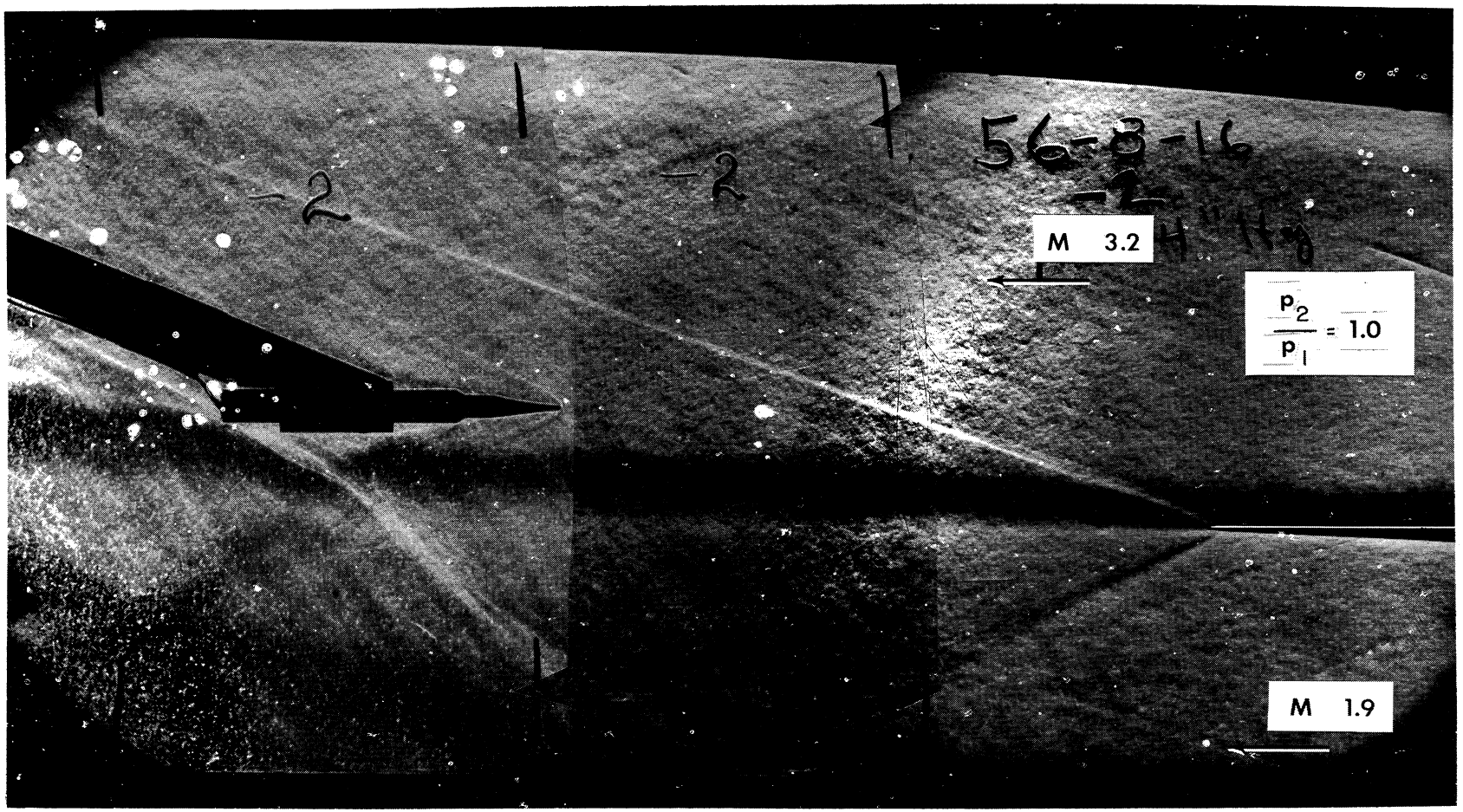

Figure 11. Schlieren photograph: $M_1 = 1.9$, $M_2 = 3.2$, $p_2/p_1 = 1.0$.

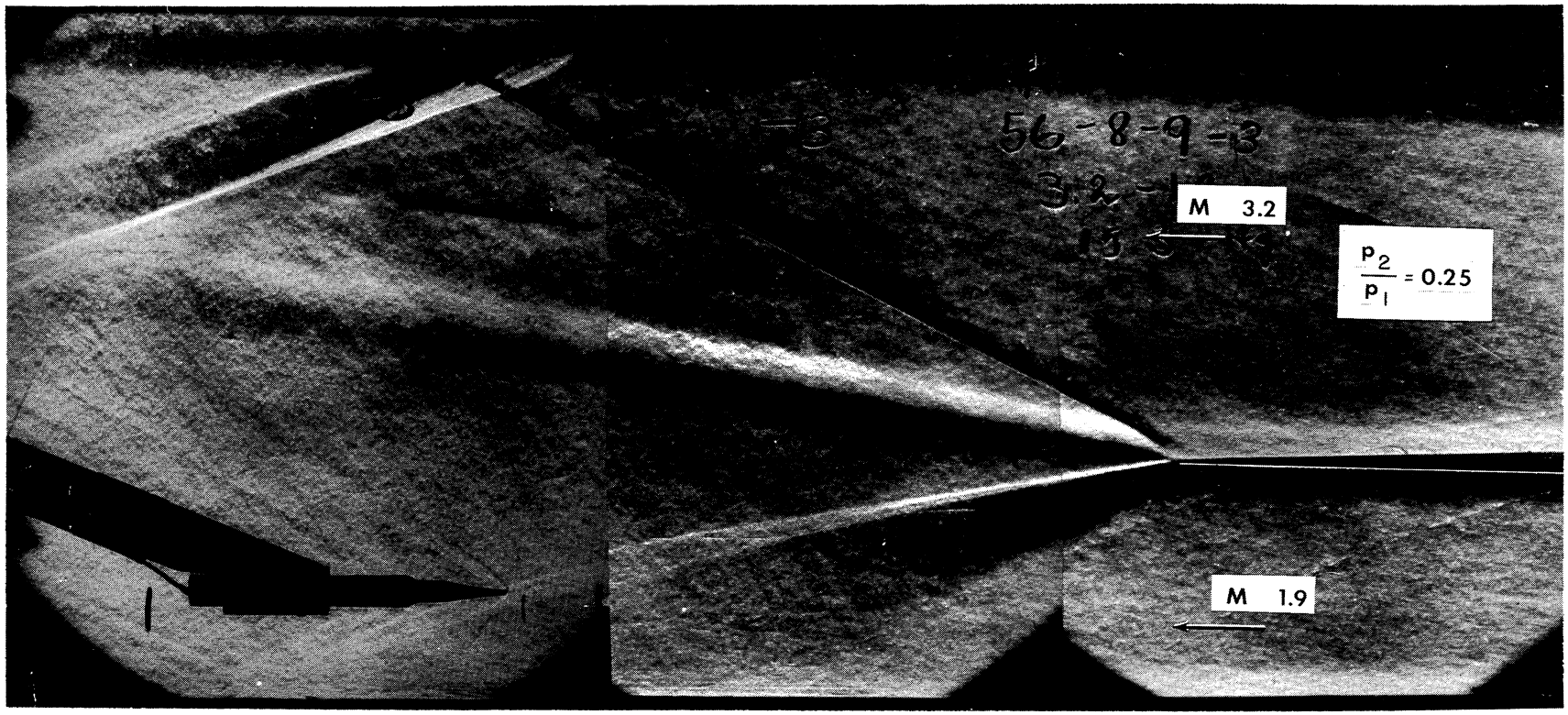

Figure 12. Schlieren photograph: $M_1 = 1.9$, $M_2 = 3.2$, $p_2/p_1 = .25$.

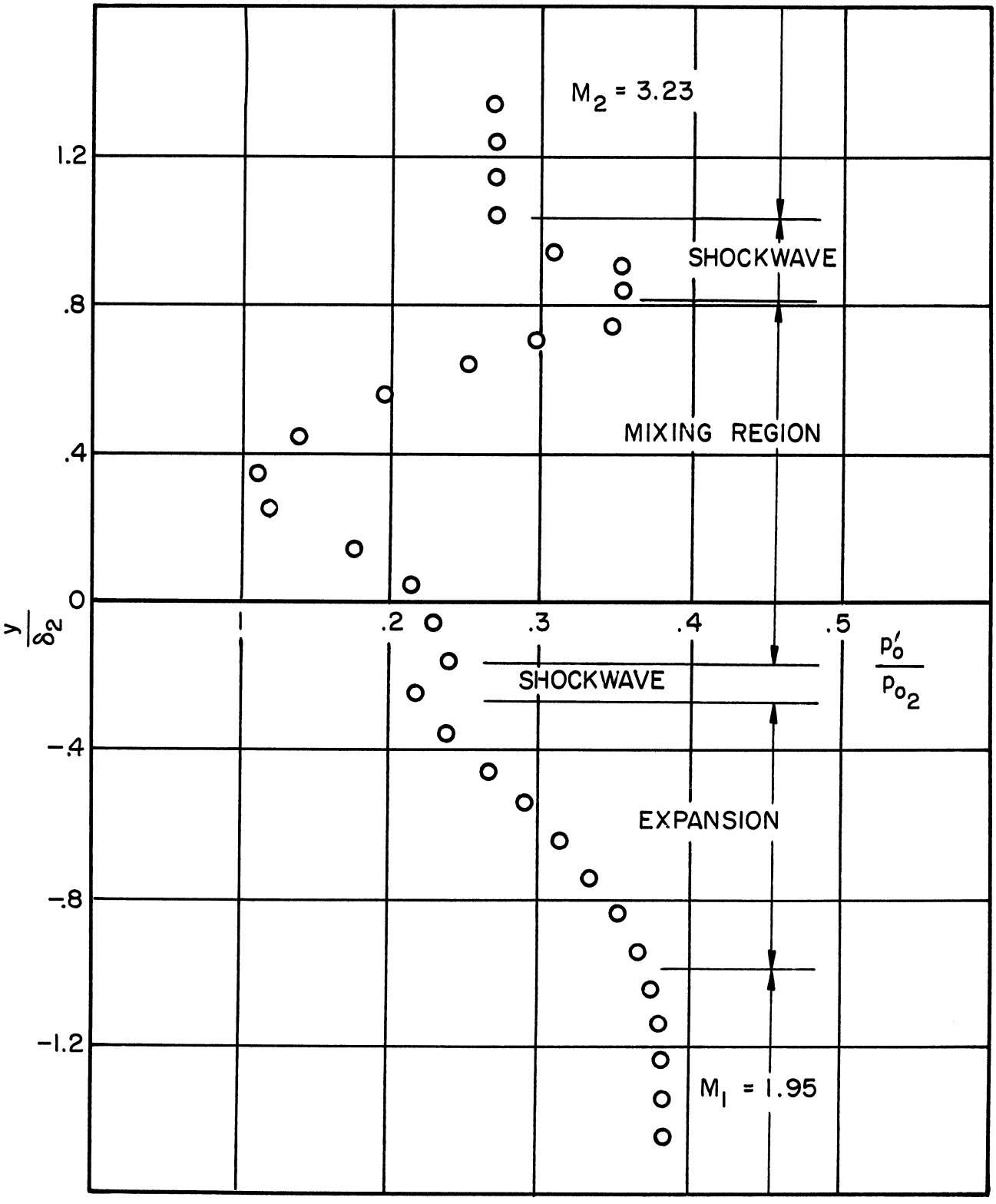

Figure 13. Total pressure profile near lip.

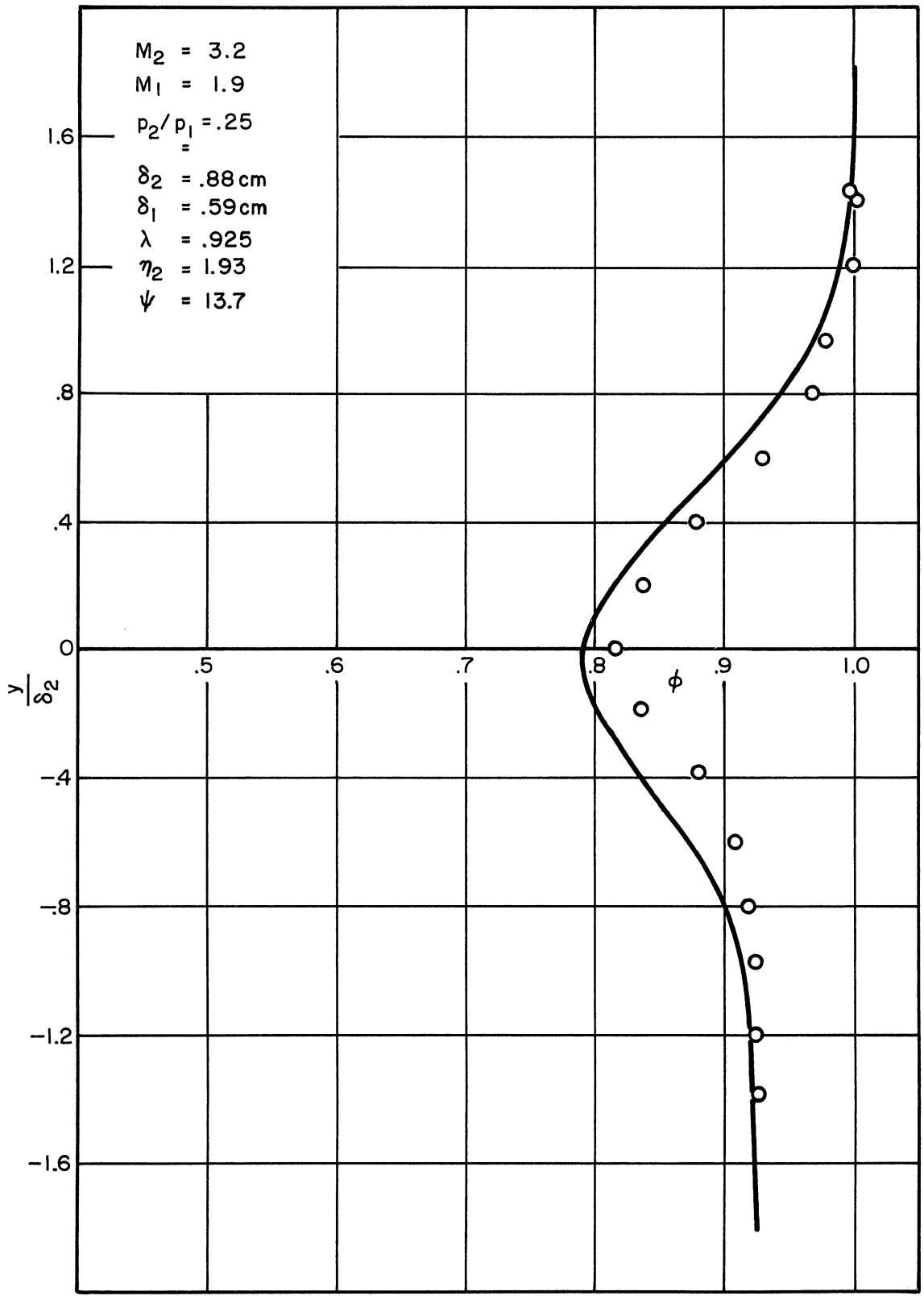

Figure 14. Theoretical and experimental velocity profiles: $M_1 = 1.9$, $M_2 = 3.2$, $p_2/p_1 = .25$.

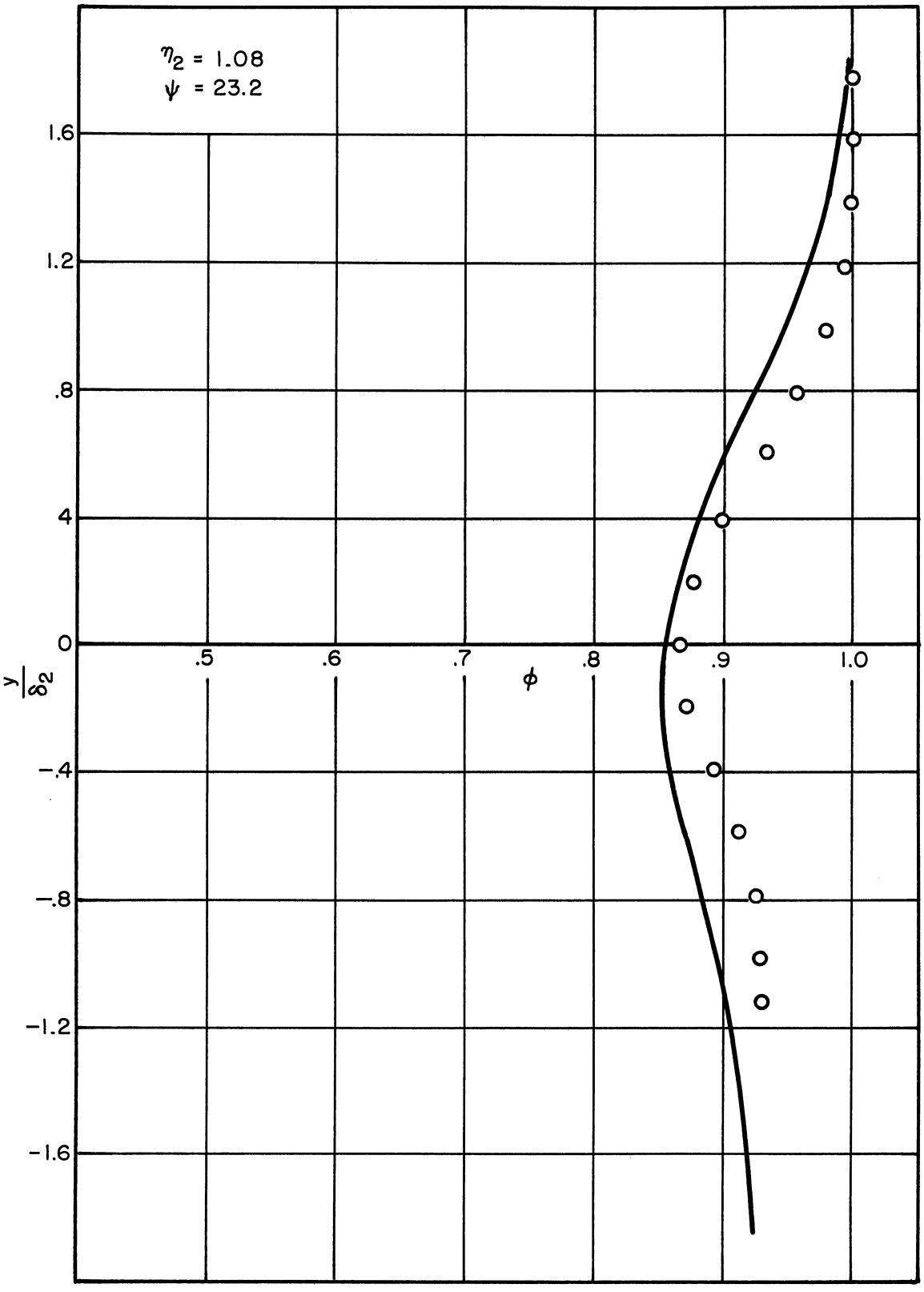

Figure 14. Continued.

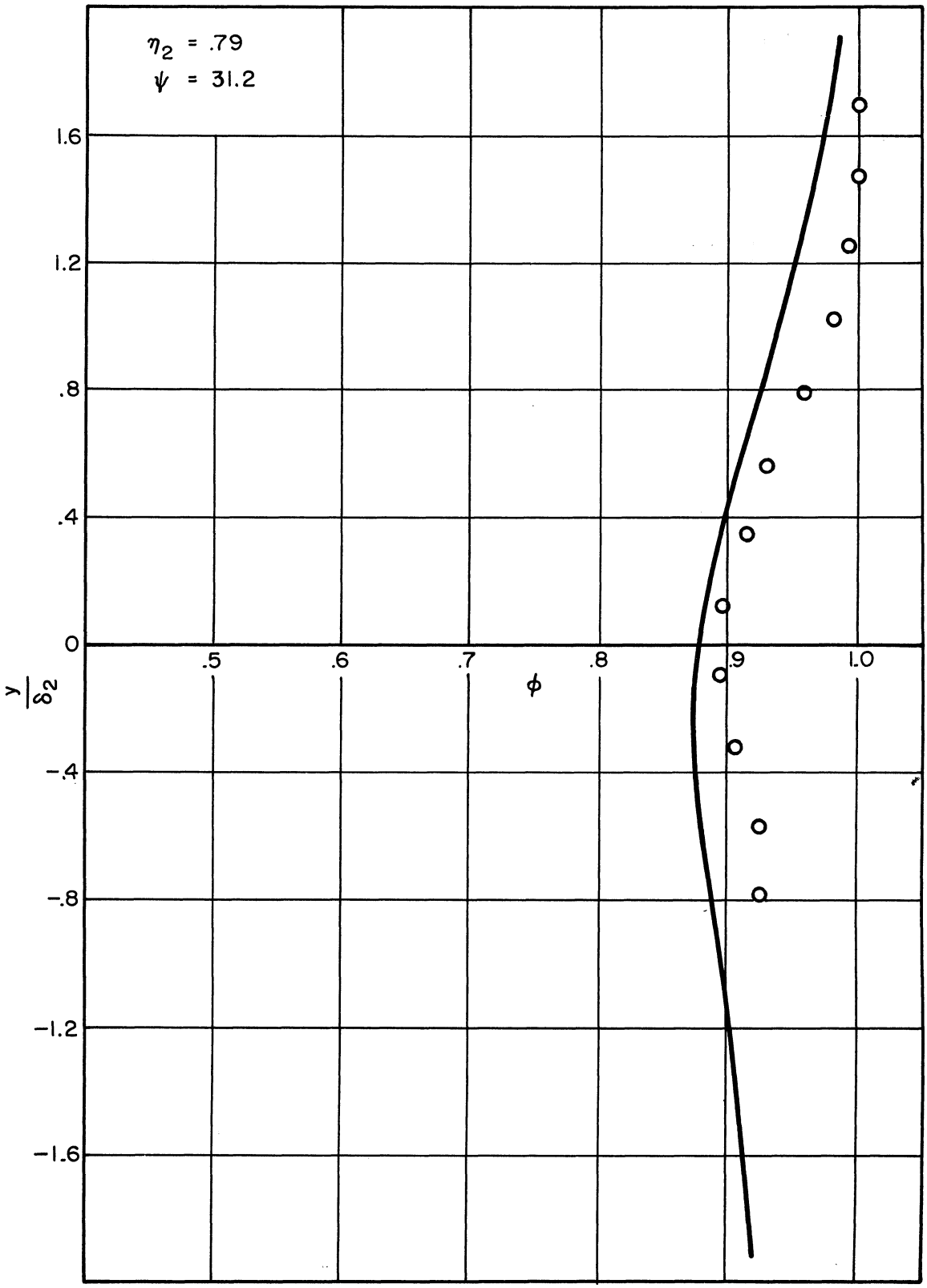

Figure 14. Concluded.

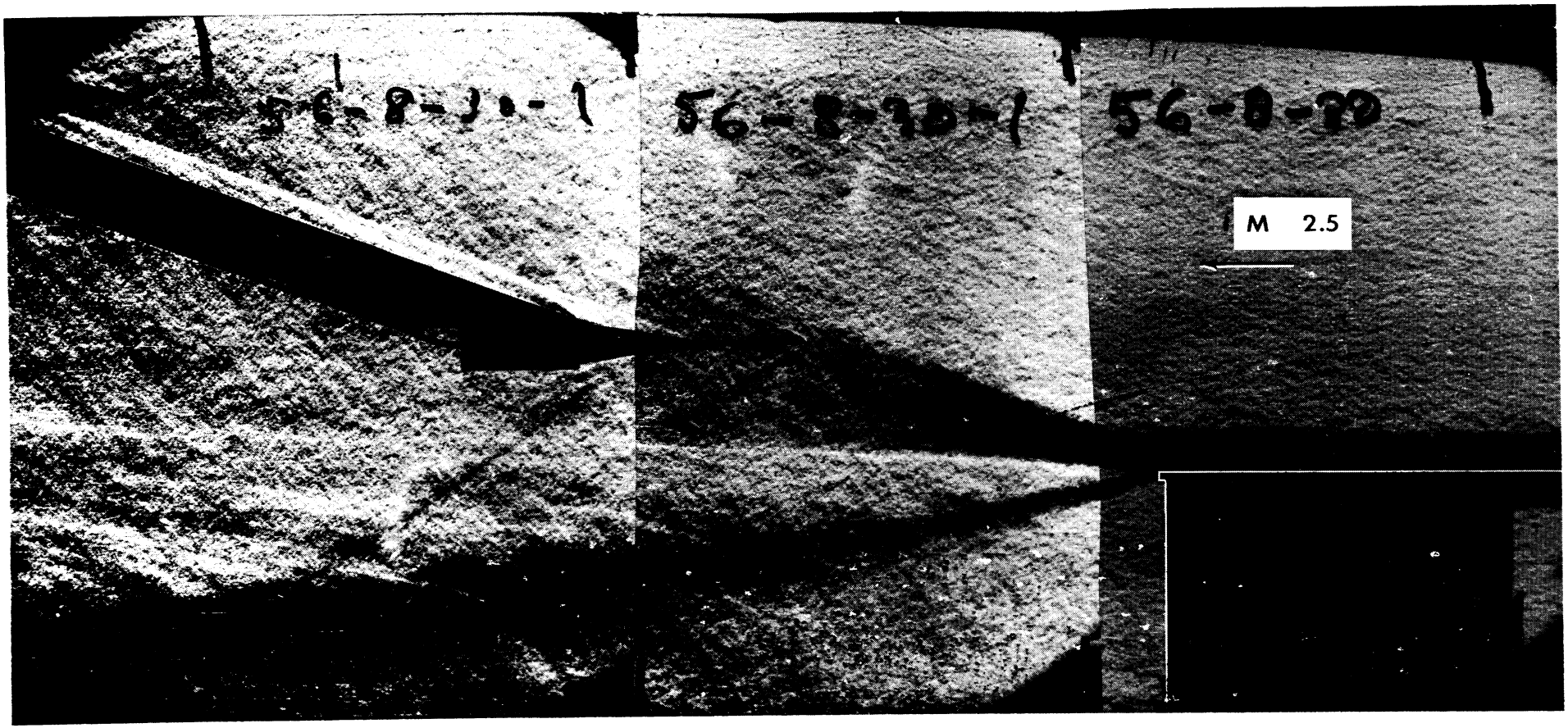

Figure 15. Schlieren photograph: $M_1 = 0$, $M_2 = 2.5$.

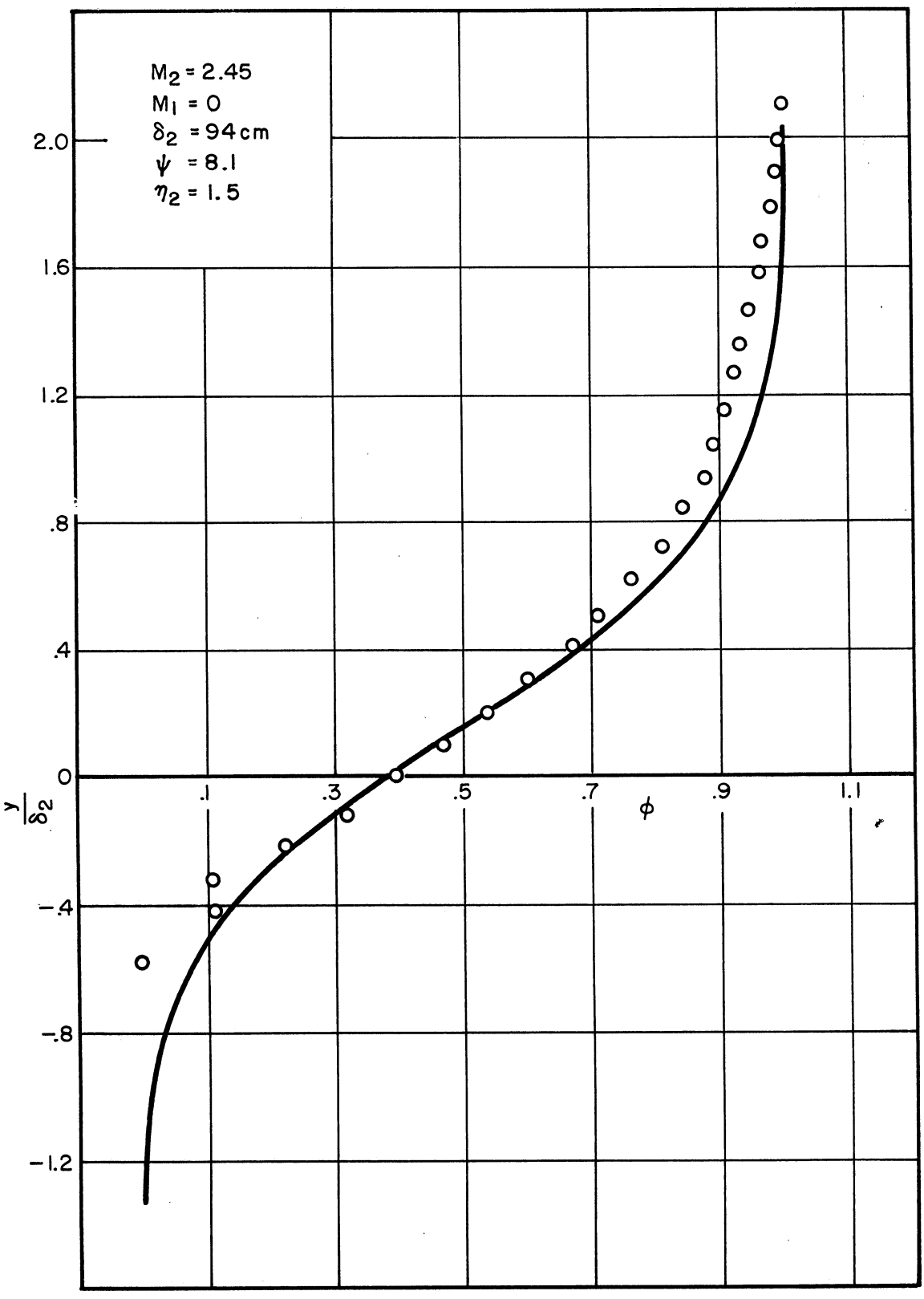

Figure 16. Theoretical and experimental velocity profiles: $M_1 = 0$, $M_2 = 2.5$.

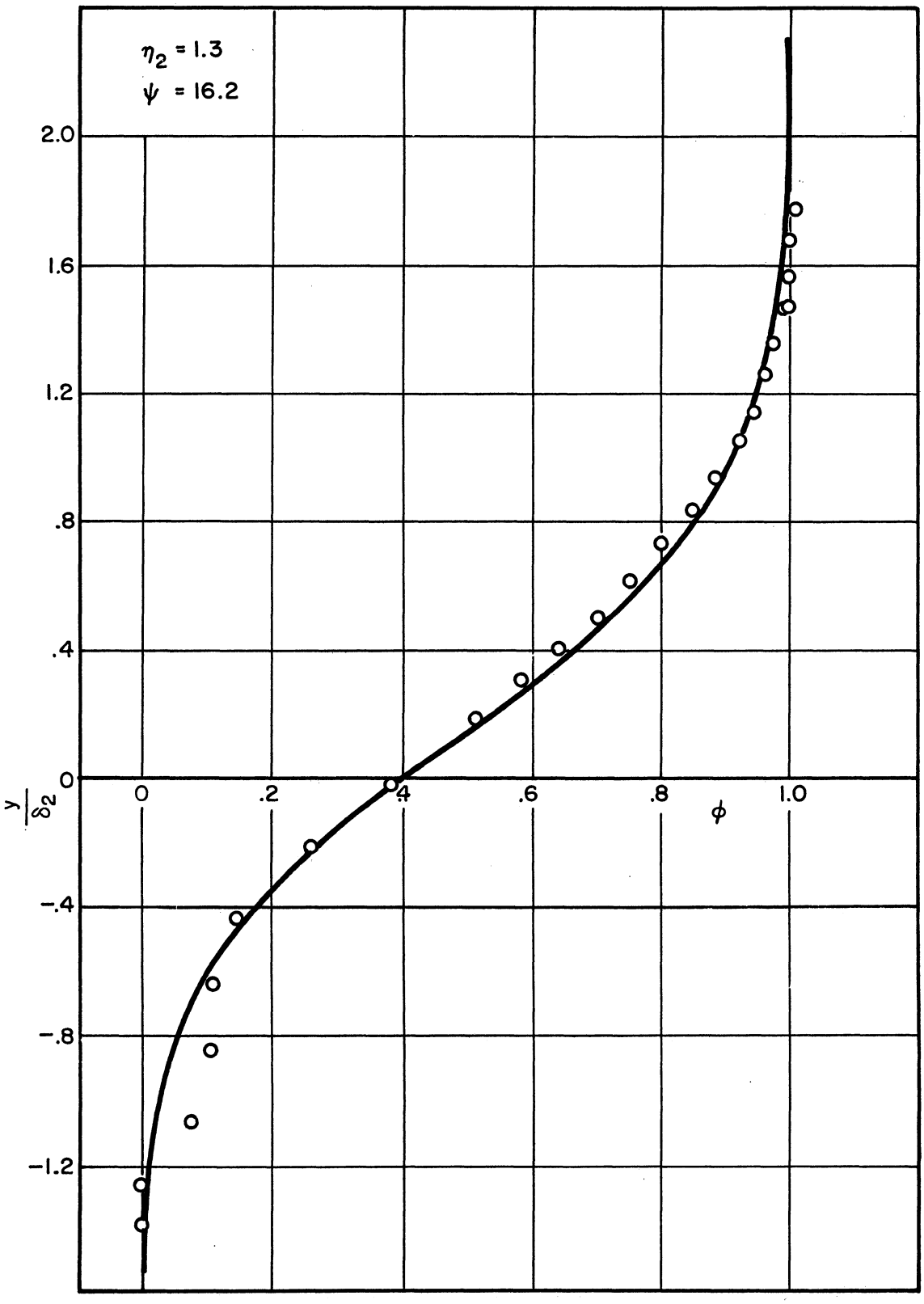

Figure 16. Concluded.

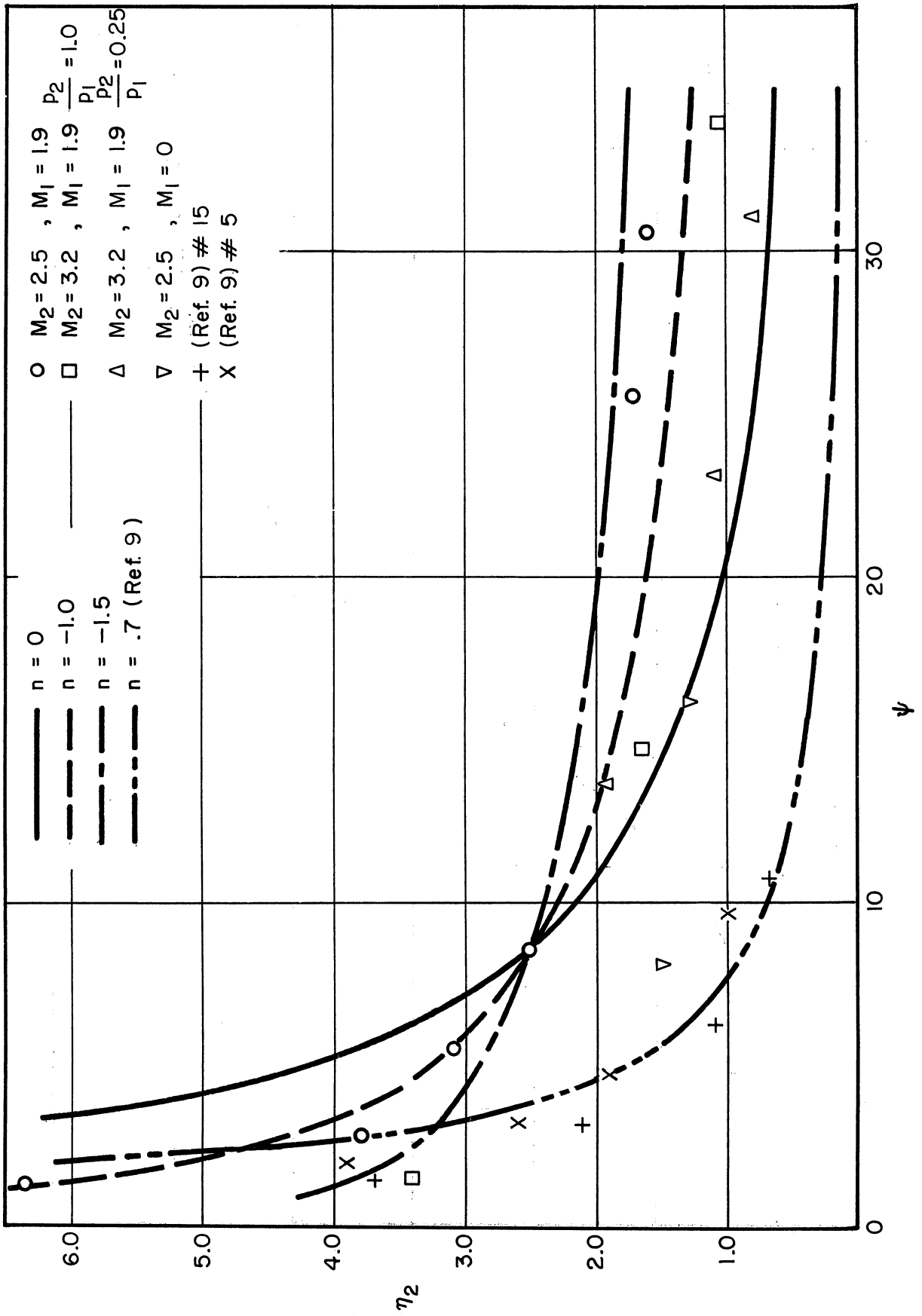

Figure 17. Plot of η_2 vs ψ for all configurations.

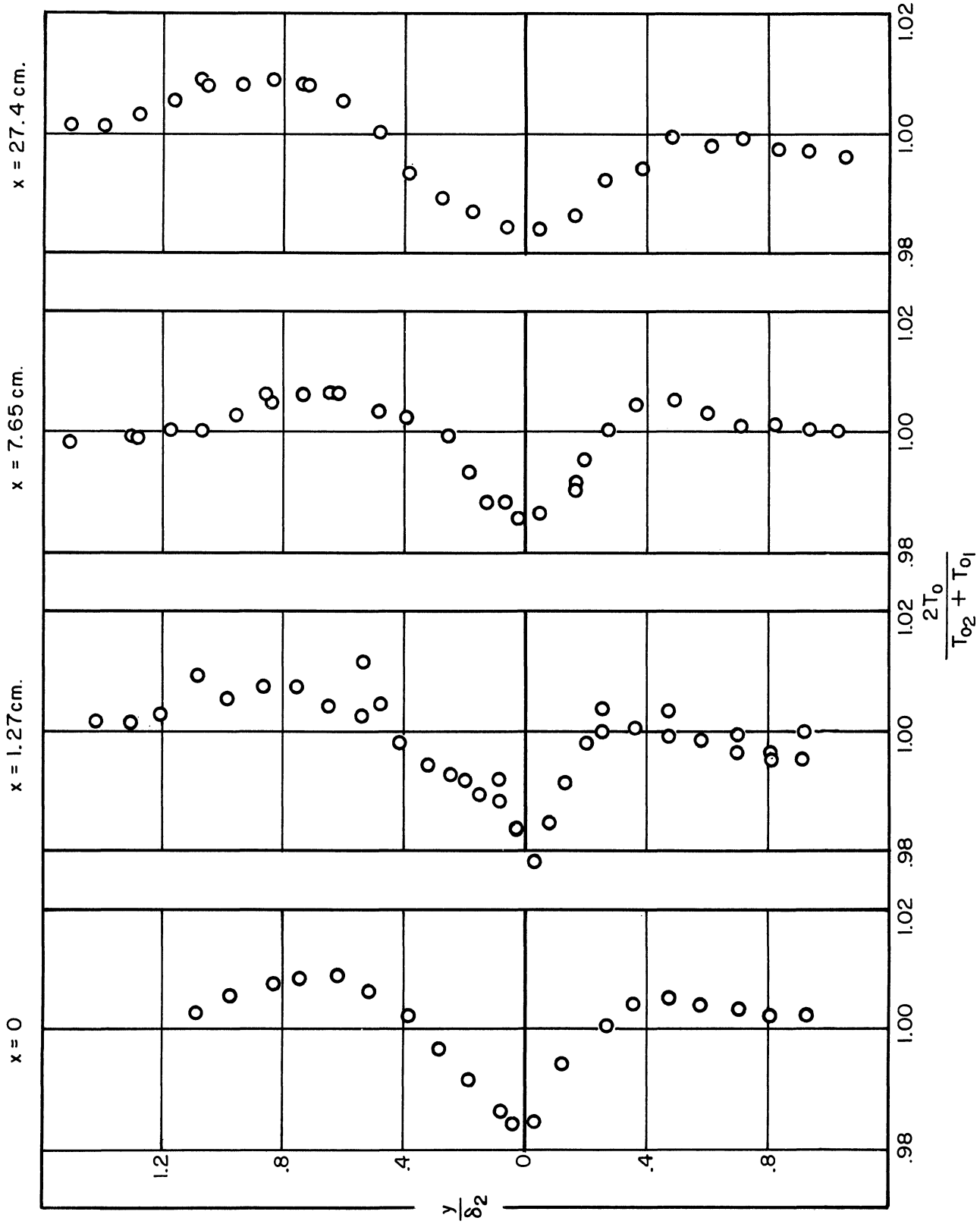

Figure 18. Stagnation-temperature profiles: $M_1 = 1.9$, $M_2 = 2.5$, $p_2/p_1 = 1.0$.

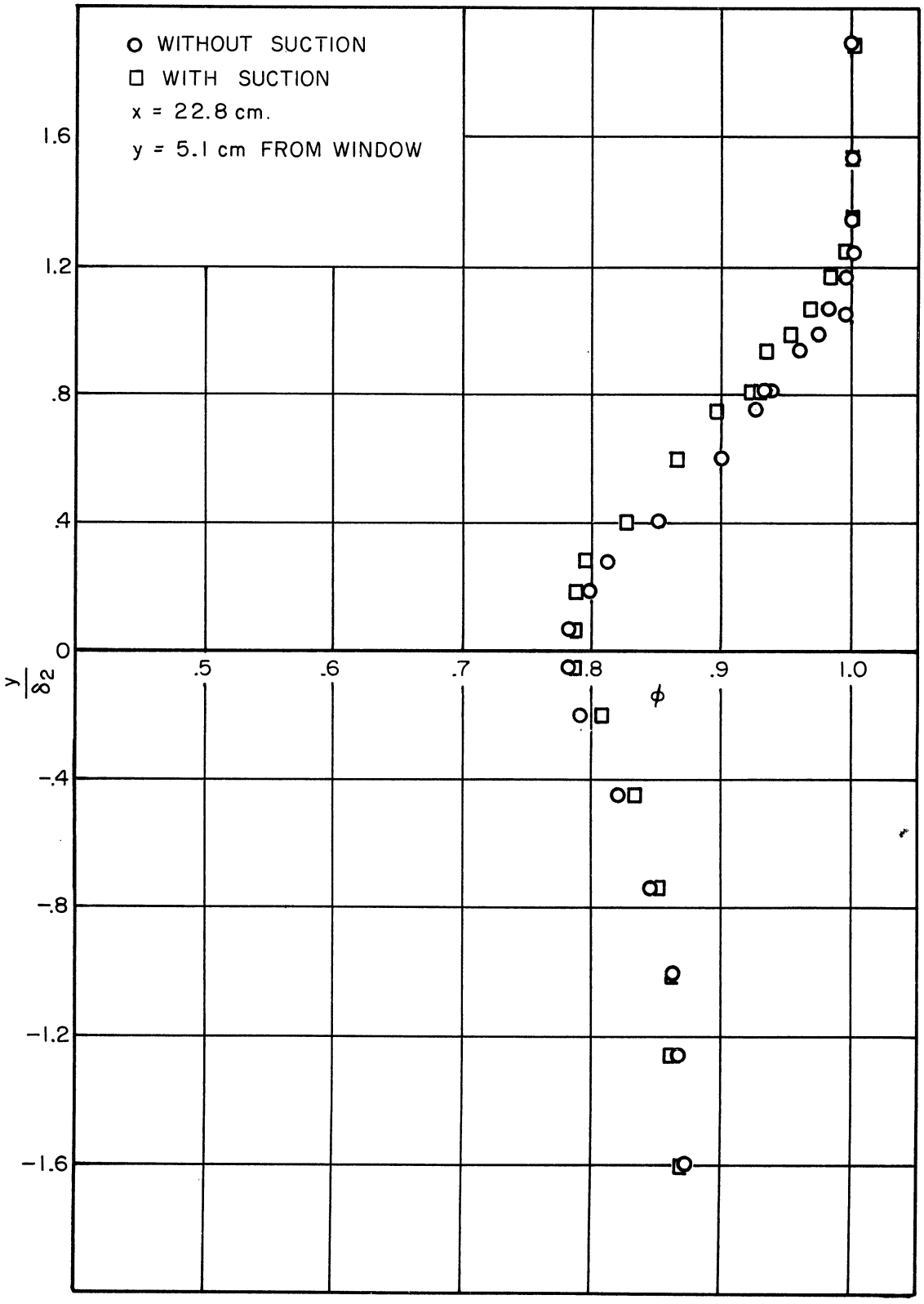

Figure 19. Experimental velocity profiles with and without suction.

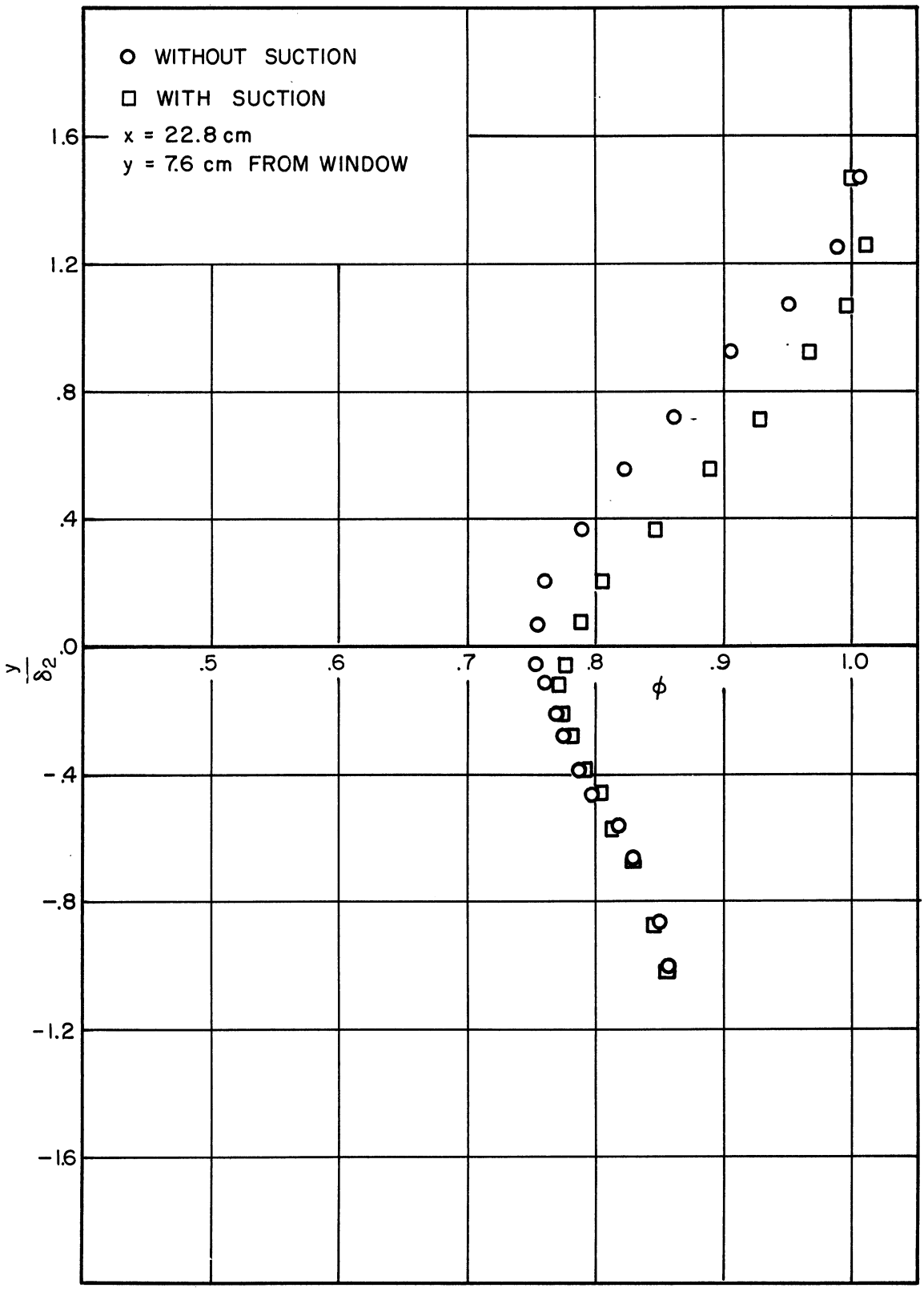

Figure 19. Concluded.